The Utility of Total Lightning in Diagnosing Single-cell Thunderstorm Severity in the Central Appalachian Mountains Region

Paul Miller

Thesis submitted to the faculty of the Virginia Polytechnic Institute and State University
in partial fulfillment of the requirements for the degree of

Master of Science
In
Geography

Andrew W. Ellis, Committee Chair
David F. Carroll
Stephen J. Keighton

April 2, 2014
Blacksburg, VA

Keywords: Total lightning, single-cell thunderstorm, pulse thunderstorm, severe weather

The Utility of Total Lightning in Diagnosing Single-cell Thunderstorm Severity in the Central Appalachian Mountains Region

Paul Miller

ABSTRACT

Recent severe weather research has examined the potential role of total lightning patterns in the severe thunderstorm warning-decision process although none to-date have examined these patterns in explicitly weak-shear environments. Total lightning flashes detected by the Earth Networks Total Lightning Network (ENTLN) during the 2012-13 convective seasons (1 May – 31 August) over a region of the Central Appalachian Mountains were clustered into likely discrete thunderstorms and subsequently classified as either single-cell or multicell/supercell storm modes. The classification of storms was determined using a storm index (SI) which was informed by current National Weather Service (NWS) identification techniques. The 36 days meeting the minimum threshold of lightning activity were divided into 24 lightning-defined (LD) single-cell thunderstorm days and 12 LD multicell/supercell days. LD single-cell days possessed statistically significant lower 0000 UTC 0-6 km wind shear (13.8 knots) than LD multicell/supercell days (26.5 knots) consistent with traditional expectations of single-cell and multicell/supercell environments respectively.

The popular 2σ total lightning jump algorithm was applied to all flashes associated with 470 individual LD thunderstorms. The frequencies of the storms' total lightning jumps were then compared against any associated severe weather reports as an accuracy assessment. The overall performance of the algorithm among both categories was much poorer than in previous studies. While probability of detections (POD) of the 2σ algorithm were comparable to previous research, false alarm rates (FAR) were much greater than previously documented. Given these results, the 2σ algorithm does not appear fit for operational use in a weak shear environment.

Acknowledgements

This material was based upon work supported by the COMET Program of the University Corporation for Atmospheric Research (UCAR) and the National Oceanic and Atmospheric Administration's (NOAA) National Weather Service (NWS) under Grant No. Z13-99434. Any opinions, findings, conclusions, or recommendations expressed in this material are those of the authors and do not necessarily reflect the views of the COMET Program, UCAR, NOAA or the NWS. The authors thank the staff at Earth Networks, Inc. for supplying the lightning data used in this project.

Table of Contents

List of Figures

List of Tables

List of Abbreviations

AHP	Analytical hierarchy process
ANOVA	Analysis of variance
CAPE	Convective available potential energy
CDO	Climate Data Online
CG	Cloud-to-ground
CSI	Critical success index
CWA	County warning area
DEM	Digital elevation model
EDHS	Enhanced diurnal heating surface
ENLS	Earth Networks lightning sensor
ENTLN	Earth Networks Total Lightning Network
ESRI	Environmental Sciences Research Institute
ESRL	Earth Systems Research Laboratory
FAR	False alarm rate
FPM	Flashes per minute
FR	Flash rate
GLM	Geostationary Lightning Mapper
GIS	Geographic information system
hPa	Hecto-Pascal
IC	Intracloud
LD	Lightning-defined
LIS	Lightning imaging sensor
LJA	Lightning jump algorithm
LMA	Lightning mapping array
LT	Local time
MBG	Minimum bounding geometry
NCDC	National Climatic Data Center
NED	National Elevation Dataset
NLDN	National Lightning Detection Network
NOAA	National Oceanic and Atmospheric Administration
NWS	National Weather Service
NWSFO	National Weather Service Forecasting Office
POD	Probability of detection
PSD	Physical Sciences Division
SOO	Science and Operations Officer
TRMM	Tropical Rainfall Measurement Mission
USGS	United States Geologic Survey
UTC	Coordinated Universal Time
UTM	Universal Transverse Mercator
VHF	Very high frequency
VLF	Very low frequency

CHAPTER 1

INTRODUCTION

1.1 Contextualizing Severe Weather Hazards

Each year, severe weather poses a legitimate risk to the life and property of millions of individuals across the United States. With an annual average of 153 deaths attributed to destructive winds (Office of Climate 2012), no region is completely immune to the threat of hazardous weather. Economic losses from the spring 2011 tornado season alone topped $25 billion (Sreenivasan 2011), and recent natural disasters such as Hurricane Sandy (United States east coast) and Super Typhoon Haiyan (southeast Asia) further illustrate the potentially devastating consequences of meteorological disasters. With such tangible human and physical impacts, accurate forecasting and warning of these events is imperative.

The National Weather Service (NWS) defines “severe weather” based on the following three criteria: (1) winds in excess of 50 knots, (2) hail greater than one inch (2.54 cm) in diameter or (3) a tornado (Storm Prediction Center 2012). Since direct measurements of wind speeds can sometimes be difficult to obtain the NWS also accepts wind damage to trees or structures as evidence of a severe weather event. If a storm exhibits any of these criteria (or their implication via damage), a severe weather event has occurred. While this characterization addresses several common threats associated with dangerous weather, it is not a comprehensive assessment of storm hazards. In addition to the aforementioned threats, lightning and flash flooding can pose a potentially deadly threat to human lives, resulting in nearly as many deaths as the

three formal severe weather criteria. When these risks are included, weather-related deaths per year jump to 268 in the United States (Office of Climate 2012).

According to its mission statement, the NWS issues “weather, hydrologic, and climate forecasts and warnings for the United States, its territories, adjacent waters and ocean areas, for the protection of life and property and the enhancement of the national economy” (National Weather Service 2012). Vital to the mission of the NWS is the ability to accurately warn and forecast the extreme events discussed above. Unfortunately, current NWS severe thunderstorm warnings do not consistently verify with observed conditions, demonstrating the need for enhanced weather forecasting techniques and technologies targeted at accurately predicting meteorological phenomena.

1.2 Contextualizing Thunderstorm Mode

Severe weather researchers have long benefited from the stratification of storms by mode, especially in the context of storm severity. It is well-acknowledged that the form of convective storms varies as characterized by longevity, degree of severity, mode of propagation, intensity of rainfall (Weisman and Klemp 1982), areal extent (e.g., Austin and Houze Jr. 1972), and therefore, their radar signature (e.g., Smith et al. 2012a). Taken together, these traits have given rise to conceptual models describing a set of storm modes that includes three broad categories: single-cell, multicell, and supercell storms (Weisman and Klemp 1982). However, for either of these storm modes there can be substantial variation in their characteristic traits. In this respect, explicitly categorizing and defining storm mode is a difficult task, prompting the suggestion of a continuous spectrum of storm modes (Weisman and Klemp 1982, 1984).

The most unorganized convective mode, single-cell ordinary thunderstorms, is generally defined as a storm forming in an environment characterized by weak vertical wind shear (< 10 m s^{-1}; Markowski and Richardson 2010). Although known to form in atmospheres possessing only a few hundred joules per kilogram (J kg^{-1}) of convective available potential energy (CAPE), single-cell thunderstorms capable of producing severe weather, also termed “pulse” storms, often require CAPE greater than 2000 J kg^{-1} (Markowski and Richardson 2010). While a true single-cell storm is relatively uncommon (Byers and Braham 1949), the disorganized mode that is referenced is prevalent during the warm season across much of the eastern United States.

Multicellular convection, a more organized form of ordinary convection, is composed of ordinary cells whose outflows initiate new ordinary cells with the assistance of atmospheric wind shear (Markowski and Richardson 2010). While the individual cells are ordinary, the multicell cluster can last for hours and easily produce hazardous weather. Supercell thunderstorms, the most organized convective mode, are a non-ordinary form of convection in which strong atmospheric wind shear enables an individual cell to last for hours (Markowski and Richardson 2010).

Discernment of convective mode is a complicated task given the commonalities and overlap in the different characteristics of storm structures (Weisman and Klemp 1982, 1984). However, its inclusion within the broader conversation of severe weather hazards has proven a fruitful and worthwhile addition over the last several decades (Smith et al. 2010). A common focus of the role of storm mode is the likelihood and type of severe weather hazard that each mode supports. Numerous studies have ventured to

document the types of storm environments that will support a given mode (e.g., Csirmaz et al. 2013; Thompson et al. 2007) as well as the subsequent severe weather events they produce (e.g., Smith et al. 2012a, b). Operational forecasters frequently appeal to these findings while formulating their forecasts, believing that a prior knowledge of storm mode will allow for a more accurate prediction of severe weather events.

Since the behavior and intensity of convective modes can vary so widely, it is wise to investigate severe weather forecast accuracy as a function of storm mode. The results of Guillot et al. (2008), which found distinct variations in NWS severe weather warning accuracy between storm modes, suggest that such a consideration is not only wise but necessary. Thus, as new weather prediction technologies become available, evaluating their comparative performance across the spectrum of convective modes should be a point of emphasis.

1.3 The Emergence of the "Total Lightning Jump"

One such emerging technology, total lightning detection, has been greatly facilitated by the recent establishment of ground-based very high frequency (VHF) lightning detection networks. Based on the results of several pioneering total lightning studies, the "total lightning jump" has emerged as a focal point among severe weather researchers. Total lightning, which is the sum of intracloud (IC) and cloud-to-ground (CG) lightning, occurs in much greater quantities than CG lightning (e.g., Boccippio et al. 2001; Goodman et al. 1988; Livingston and Krider 1978; MacGorman et al. 1989, 2011) and offers a much more comprehensive insight toward storm electrification. Many studies have documented these total lightning jumps – a term referencing sharp

increases in the total lightning flash rate of thunderstorms (i.e., a “jump”) just prior to the onset of severe weather at the surface (e.g., Darden et al. 2010; Gatlin and Goodman 2010; Goodman et al. 1988; Goodman et al. 2005; MacGorman et al. 1989; Rudlosky and Fuelberg 2013; Schultz et al. 2009, 2011; Williams et al. 1999).

With the first formulation of a lightning jump algorithm (LJA) by Gatlin and Goodman (2010) and refined by Schultz et al. (2009, 2011), there exist several definitions for the increase in total flash rate that constitutes a jump. The “2σ algorithm” (Schultz et al. 2009, 2011), so named for its requirement that the current flash rate exceed two standard deviations of the running mean flash rate, was shown to be the most reliable among all the tested versions of an LJA (Schultz et al. 2009) and has been tentatively adopted by researchers as the standard version of the algorithm (Rudlosky and Fuelberg 2013; Schultz et al. 2011).

1.4 Identifying the Need for Further Research

Nowhere is a thunderstorm severity forecast tool more needed than in environments characterized by weak wind shear. Single-cell thunderstorms are a frequent summertime forecasting challenge in regions where warm and moist air masses are common, such as in much of the eastern and southeastern United States, including Southwest Virginia. While these storms can occasionally produce brief episodes of severe weather, perhaps their greatest consequence lies in the challenge they pose to the warning-decision process. Unfortunately, operational forecasters possess few tools by which to warn for the severity of a single-cell storm, making it difficult to offer advanced warning. Currently, forecasters rely heavily upon radar

observations that can only identify potential single-cell severity a few minutes before the effects are felt at the surface.

Consequently, research has shown that strong and severe single-cell storms are consistently under-detected and falsely-warned (Guillot et al. 2008) creating a frustrating combination of frequency and difficulty. According to Guillot et al. (2008), the probability of detection (POD) for severe weather associated with pulse-type convection as well as the false alarm rate (FAR) for warnings issued on these storms are roughly 60% (compared to 80% POD and 40% FAR for isolated supercells). Meanwhile, lead times are roughly six minutes shorter for pulse-type storms than isolated supercells (Guillot et al. 2008). An increase in pulse-type thunderstorm warning accuracy as well as the development of new, reliable forecasting tools are welcome areas of improvement for the NWS.

With total lightning observations expected to become widely available among operational forecasters upon the planned launch of the GOES-R satellite in late 2015 (Fierro et al. 2014), a reliable LJA holds the potential to improve both the probability of detection (POD) and false alarm rate (FAR) of severe weather warnings. However, previous LJA studies have given little focused attention to the convective regimes in which the storms form, and consequently, overlook the role of convective mode. While some have included brief discussions of the algorithm's performance among different storm modes (Goodman et al. 2005; Schultz et al. 2011), no research to-date has provided detailed documentation of an LJA's performance in the context of a single specific convective environment. Consequently, the purpose of this study is to assess

the transferability of the 2σ algorithm to weakly-sheared atmospheres that host disorganized single-cell thunderstorms during the summer months.

Given these uncertainties, this thesis will address the following basic question: is there a relationship between total lightning trends and storm severity in weak-shear environments? Additionally, the study will also consider the following applied research question: can the 2σ total lightning jump algorithm be used as an effective operational forecasting tool in weakly sheared atmospheres? To inform the above research questions, this thesis will consider total lightning flashes occurring during the 2012 and 2013 convective seasons (1 May – 31 August) within the central Appalachians region of the United States. Flashes will be clustered into thunderstorms and classified as either single-cellular or multicellular/supercellular based on their spatial and temporal characteristics. Finally, the 2σ algorithm will be applied to all clusters of flashes and compared against any associated severe weather reports with special attention paid to the single-cell clusters.

This thesis will break its evaluation into four distinct sections – one section of data explanation and three sections of analysis. The data section (Ch. 3) will contain a discussion of all data sources utilized by all three chapters of analysis. Any data sources unique to only one stage of analysis will be discussed within that relevant section. The three sections of analysis will broach the following topics respectively: the process of single-cell thunderstorm identification for 2012 (Ch. 4), the expansion of total lightning observations to 2013 and the spatial distribution of all 2012 and 2013 single-cell thunderstorms within the study domain (Ch. 5), and the performance of an LJA

among 2012-13 single-cell thunderstorms (Ch. 6). Figure 1 outlines the basic flow of the thesis as described above. These questions will not only consider the behavior of total lightning frequency in this environment, but they will also evaluate the forecasting implications of any evident patterns.

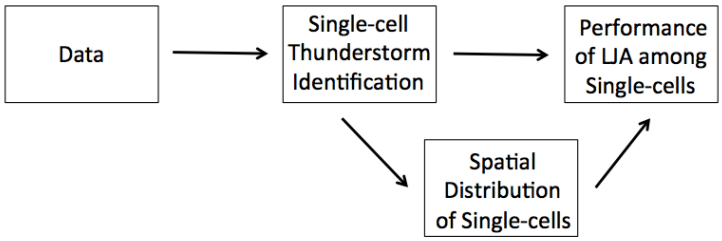

Figure 1. Flow of topics within thesis. The "spatial distribution of single-cells" is offset since it contributes to the thesis by expanding the temporal domain of the study to include 2013 for use in the LJA analysis, but the spatial distribution analysis it completes does not contributed directly to the research questions posed by the thesis.

CHAPTER 2

Literature Review

2.1 A Brief History of Lightning Detection

Lightning poses serious threats to human life and infrastructure, a fact that has long been acknowledged by scientists, policy-makers and the general public. Lightning not only constitutes a direct threat to human life when it strikes at ground level, but it also disrupts power grids and induces electromagnetic interference in electronics (Cummins and Murphy 2009). High-end estimates of lightning-related damages range between $4-5 billion annually in the United States alone (Rauber et al. 2008). As a reaction to these concerns, the development of lightning locating systems began as early as the 1920s (Cummins and Murphy 2009).

Lightning sensors take advantage of a basic and long-studied characteristic: the emission of electromagnetic pulses by lightning flashes (Cummins and Murphy 2009). As the atmosphere breaks down prior to the establishment of an IC lightning channel, a very high frequency (VHF) electromagnetic emissions occurs (Cummins and Murphy 2009). Oppositely, long transmissions of high current along existing channels produce emissions with a very low frequency (VLF; Cummins and Murphy 2009). The latter of these emissions is largely characteristic of the powerful return strokes observed in CG lightning flashes (Cummins and Murphy 2009). Therefore VHF emissions are evident with all lightning flashes as they initially form a channel of current, but VLF emissions are typically representative of CG flashes (Cummins and Murphy 2009). The distinction

and discrimination between VHF and VLF electromagnetic emissions forms the basis of IC and CG lightning detection.

The frequency of the emission also contributes to very distinct differences in how the emissions propagate through the atmosphere. VLF emissions, reflected by the ionosphere, can travel very long distances while VHF emissions must be observed much closer to the source (Cummins and Murphy 2009). Consequently, CG lightning detection has traditionally been much more practical over large areas. Despite the long legacy of lightning research, sensor and circuitry limitations to large-scale implementation of a lightning detection network have only been overcome within the last 30 years (Cummins and Murphy 2009). The best known of these systems is the National Lightning Detection Network (NLDN), which began operation in 1989 with a network of over 100 sensors (Cummins and Murphy 2009). The greater than 20-year archive of NLDN observations has been extensively utilized by university researchers and operational weather forecasters.

Since 2009 the Earth Networks Total Lightning Network (ENTLN) has observed total lightning flashes across the continental U.S. (Earth Networks 2012). Although the NLDN has catalogued flashes for a much longer time period, it only reliably detects flashes that make contact with the ground (Cummins and Murphy 2009). Since it is now known that CG flashes represent only a fraction of lightning activity (e.g., Goodman et al. 1988; MacGorman et al. 1989; Montanya et al. 2009), total lightning must be considered to gain the most complete picture of storm intensity. While regional lightning mapping arrays (LMAs) have possessed this ability for some time, the large-scale

observation of both flash species has only recently become feasible with the implementation of the ENTLN (Earth Networks 2012).

Though the NLDN has certainly proven invaluable over the past several decades, the CG flashes it identifies nonetheless only represent a fraction of the total lightning production of a storm. To gain a more holistic picture of lightning activity across a much larger domain, government agencies have endeavored to develop total lightning flash sensors for inclusion on spaced-based observation platforms. Two attempts worthy of note include the Lightning Imaging Sensor (LIS) mounted within the Tropical Rainfall Measuring Mission (TRMM) satellite and the Global Lightning Mapper (GLM) slated to be launched onboard the National Oceanic and Atmospheric Administration's (NOAA) GOES-R satellite in late 2015 (Fierro et al. 2014). With the advent of the ENTLN and the impending GOES-R satellite, researchers are laboring to extract the full forecasting potential from newly available total lightning observations.

2.2 The Relationship Between Total Lightning and Cloud-to-Ground Lightning

As soon as reliable VHF detection networks commenced operation (albeit on small scales), researchers began comparisons between IC and CG flash behavior (MacGorman et al. 2011; Montanya et al. 2009; Williams et al. 1999; Williams et al. 1989). While it is certainly reasonable to believe that total lightning provides a much more complete representation of storm intensity, many studies have attempted to verify this experimentally. Their results have shown that around 80% of all lightning flashes occur completely within the cloud (Rauber et al. 2008), and at times this proportion can climb to 95% (Goodman et al. 1988). Additionally, pulse-type thunderstorm flash rates in

the cloud have been observed to approach 100 min^{-1} while CG flash rates remain near 5 min^{-1} (Goodman et al. 2005).

Not only does IC lightning dominate the proportion of total lightning, but it is almost always observed before the first CG flash (MacGorman et al. 2011). Interestingly, the same study observed that a small subset of intense high flash rate storms required noticeably longer to produce their first CG flash (MacGorman et al. 2011) demonstrating the temporal advantage of total lightning observation. With the majority of first observable flashes and the vast majority all subsequent flashes occurring in the cloud, it is imperative to develop a solid operational understanding of total lightning trends.

The maximum flash rates of the two lightning species also been observed to vary temporally. Peak IC flash rates tend evolve in phase with storm updraft (Goodman et al. 1988), meaning that increases/decreases in total lightning flash rate signal strengthening/weakening of the updraft, respectively. During the initial stages of the storm when the updraft is strengthening, IC lightning is far more frequent than CG flashes (Williams et al. 1989). However, as the storm matures CG flashes have been observed to outnumber IC by 20 CG flashes to zero IC flashes during short periods near the end of the storm's lifetime (MacGorman et al. 1989). MacGorman et al. (1989) also documented widely varying CG flash tendencies between two supercell storms of similar intensity. In the two storms that were observed, one exhibited low, yet stable rates while another displayed large, highly variable rates (MacGorman et al. 1989). These trends suggest that while CG lightning (in contrast to total lightning) is

nonetheless an indicator of storm intensity, it displays a weaker correlation to the observable evolution of a thunderstorm.

2.3 The Relationship Between Total Lightning and Storm Severity

In one of the earliest studies to relate total lightning to subsequent storm severity, MacGorman et al. (1989) observed total lightning trends throughout the evolution of a tornadic supercell thunderstorm. Total lightning flash rates were compared against the storm's mesocyclone strength, CG flash rates, and radar reflectivity (MacGorman et al. 1989). The results showed that the total flash rate peaked near the time of the tornado while the CG flash rate exhibited no connection to the manifestation of severe weather. The total lightning peak prior to the occurrence of severe weather soon became a common result of later studies (Williams et al. 1999; Williams et al. 1989). Lead times between the sharp total lightning increases and ensuing severe weather ranged from 4 minutes (Goodman et al. 1988) to 20 minutes (Williams et al. 1999). In a 711-storm sample, total lightning jumps provided a 20.65-minute lead time on observed severe weather (Schultz et al. 2011).

As total lightning gained credibility, the term "lightning jump" was first adopted to describe the sharp increase in the time derivative of total flash rate observed prior to severe weather (Williams et al. 1999). However, it was not until 2009 that serious attempts were made to transform the lightning jump into an operational forecasting tool (Schultz et al. 2009). Recent research has centered upon the development of a total lightning jump detection algorithm (Gatlin and Goodman 2010; Schultz et al. 2009) – a clear definition for the total lightning trends that constitute a jump. These algorithms

ingest real-time total lightning data so that jumps, as defined by the algorithm (Gatlin and Goodman 2010), may be automatically identified. Two studies evaluated several variations of the algorithm by manipulating the relationship between the standard deviation and mean of the running flash rates (Schultz et al. 2009) as well as the length of the moving interval (Gatlin and Goodman 2010). Schultz et al.'s (2009) evaluation revealed the best performing algorithm for identifying potential severity defined a jump as when a storm's most recent running flash rate exceeded two standard deviations (2σ) above the running means of the preceding twelve minutes.

The ultimate goal of these diagnostic algorithms (and/or human forecasters) is to correctly identify all storms that eventually produce severe weather and additionally, refrain from incorrectly identifying non-severe storms as severe. Operationally, these performance parameters are measured by the values POD and FAR. Ideally forecasters, or a forecasting algorithm, would achieve a 100% POD and 0% FAR. While falling short of perfection, Schultz et al.'s (2009) 2σ algorithm nonetheless yielded an impressive 87% POD and 33% FAR. A follow-up study that was conducted two years later achieved very similar results (79% POD, 36% FAR) with a much larger 711-storm sample size (Schultz et al. 2011). These POD and FAR values exceed current NWS performance numbers (Schultz et al. 2009) illustrating the potential utility of total lightning in the warning-decision process.

2.4 The Relationship Between Total Lightning and Single-cell Storm Severity

As total lightning research has gained momentum, studies have become more ambitious in terms of sample size. By virtue of expanding the number of storms and

environments analyzed, more single-cell storms have been included in recent research with one such study including over 400 single-cells (Schultz et al. 2011). While this is a promisingly large number, only 16% of the study's observed severe weather events were generated by this storm type (Schultz et al. 2011). This study highlights the frustrating challenge thwarting pulse-type storm research: while relatively frequent compared to other convective modes, a low proportion actually produce severe weather. Since the probability and intensity of severe weather is low, the idea of performing research in this environment is often neglected. However, it is for this same reason that pulse thunderstorms are a consistent forecasting challenge. Since only 1 in 4 single-cells considered by Schultz et al. (2011) produced severe weather, NWS forecasters must exercise greater skill and discretion to avoid issuing false alarms.

Pulse thunderstorms have only received specialized attention in regard to total lightning by Goodman et al. (1988). The observed storm, forming in a low shear environment, produced a total lightning peak 4 minutes in advance of near-severe wind gusts at the surface (Goodman et al. 1988), a result consistent with more organized convective modes. Other studies have utilized data from pulse storms, but grouped them into larger study samples masking any systematic lightning characteristics resulting from storm structure (Schultz et al. 2011; Williams et al. 1999; Williams et al. 1989). The assumption that all storm modes exhibit comparable total lightning trends preceding the manifestation of severe weather may indeed be true, but nonetheless must be empirically assessed.

CHAPTER 3

DATA

3.1 Total Lightning Observations

The ENTLN operates a system of 700 lightning detection sensors world-wide [S. Heckman, Senior Lightning Scientist, Earth Networks, 2013, personal communication]. The basis of the network, the Earth Networks Total Lightning Sensor (ENLS), is capable of detecting electromagnetic frequencies between 1 Hz and 12 MHz (Liu and Heckman 2011). This wide range of frequencies allows the network to locate and classify the low-frequency waveforms emitted by CG strikes as well as the high-frequency emissions of IC strikes. Waveforms detected by the ENLS are classified as either IC or CG, and subsequently grouped into flashes if they occur within 700 milliseconds and 10 km of each other (Liu and Heckman 2011). As implied by this data processing sequence, lightning flashes, which are the subject of this study, are composed of one or more strokes. In the preprocessed data obtained from the ENTLN, all detected strokes had already been combined into flashes.

In order for a flash to be formally recorded by the ENTLN, 5-8 sensors must agree on the time and location (S. Heckman, 2013, personal communication), minimizing the concern that erroneous flashes are recorded in the database. Comparisons of the ENTLN to LMAs (Carey et al. 2011) and the LIS satellite (Sloop et al. 2014), have found reasonable consistency between the data sources. The detection efficiency of the ENTLN approaches 99% for CG flashes in the eastern U.S. while the detection efficiency for IC flashes over the study area (Fig. 2) is roughly 70% (Liu and

Heckman 2011). Following an upgrade of the detection algorithm, comparisons to rocket-triggered flashes in Florida determined a median location error of 687 m (Mallick et al. 2013).

It should be noted that the ENTLN detection algorithm used to process the waveforms sensed by the ENLS was upgraded during the winter of the 2012-13. The more accurate processing of the waveforms resulted in three major systematic changes to the ENTLN detection capability: increased detection efficiency, increased strength accuracy, increased classification efficiency, and decreased location accuracy (Mallick et al. 2013). Since the algorithm upgrade increased detection efficiency and classification efficiency (Mallick et al. 2013) special selectivity must be exercised when utilizing observations before and/or after the upgrade. The detection of a greater proportion of flashes could artificially increase the observed flash rates of storms during 2013. Any Accommodations against such systematic error will be discussed in Chapters 4, 5 and 6 as relevant.

3.2 Archived Radiosonde Observations

In order to characterize the atmospheric environment in which the lightning flashes occurred, daily 1200 UTC and 0000 UTC, corresponding to 0800 and 2000 local time (LT), radiosonde data were obtained for the Blacksburg, Virginia (KRNK) launch site, located at approximately 37.2°N, -80.4°W. At an elevation of 654 m, the KRNK sounding site sits in the heart of the Appalachian Mountains near the center of the domain area (Fig. 2a). Sounding data were retrieved from the University of Wyoming upper air data distribution page (http://weather.uwyo.edu/upperair/sounding.html). While

not explicitly included by the data providers, 0-6 km wind shear (knots) was calculated by finding the magnitude of the difference of the wind vectors at the surface and an interpolated vector 6 km above the surface. A linear interpolation was performed using the wind vectors immediately below and above the 6 km level. Several studies have found 0-6 km wind shear to provide a meaningful measure of storm organization (e.g., Thompson et al. 2003). Days with sounding malfunctions were excluded from the analysis. While the 0000 UTC sounding is advantageous as a direct observation, in some cases the sounding profile may have been influenced/contaminated by convection occurring prior to this evening balloon launch.

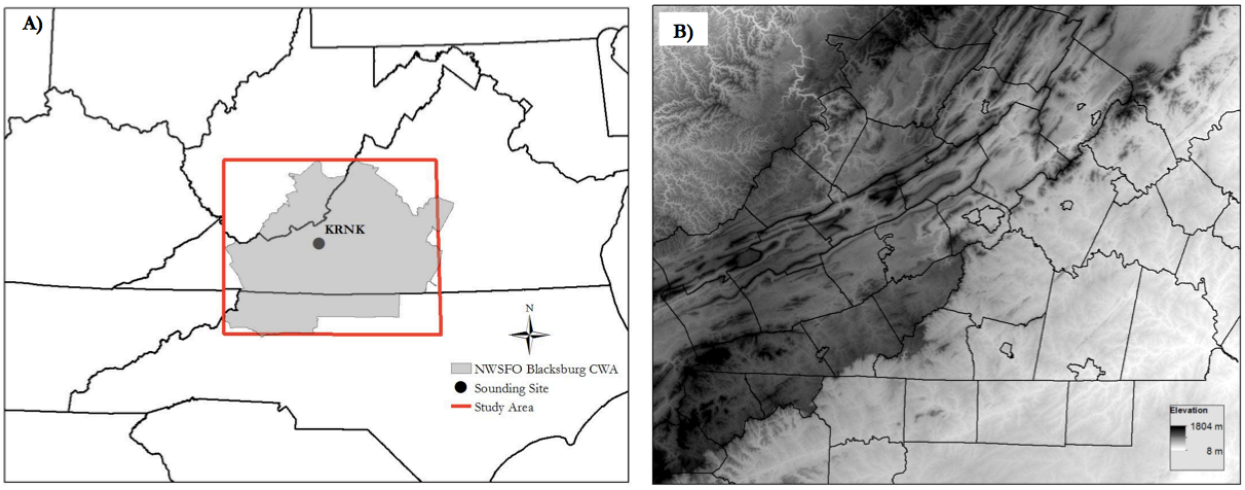

Figure 2. Study domain a) as situated within the greater Mid-Atlantic region and b) as encompassing a diversity of terrain. The domain covers roughly 75,630 km^2 with the KRNK sounding site located approximately in the center of the study area.

3.3 Other Data Sources

This thesis utilizes several other data sources in more limited capacities throughout its analysis. These data will not be discussed here, but rather, they will be addressed within succeeding chapters as relevant.

Chapter 4

A Preliminary Assessment of Using Spatiotemporal Lightning Patterns for a Binary Classification of Thunderstorm Mode

by

Paul Miller[1]

Department of Geography
Virginia Tech, Blacksburg, Virginia

[1]Corresponding author address: Department of Geography MC0115, Virginia Tech, 220 Stanger Street, Blacksburg, VA 24061. Email: paulm89@vt.edu

---

Abstract

This chapter provides a preliminary, regional assessment of the viability of using spatiotemporal lightning patterns to classify storms into single-cell versus multicell and supercell storm modes. Total lightning flashes (intracloud and cloud-to-ground flashes) occurring during the afternoon and evening of the period May through August 2012 within an area of the central Appalachian Mountains region were grouped based on their spatial and temporal characteristics using single linkage clustering. The resulting discrete thunderstorm clusters were characterized in terms of duration, motion, areal extent, and shape. These values were used to formulate four individual attribute scores representing similarity to the expected values for a typical single-cell thunderstorm. The four scores were then combined into a storm index (SI) using relative weights determined through the Analytic Hierarchy Process (AHP) performed on input from operational forecasters. Of the study days, 89 (72.4%) possessed appreciable lightning, of which 36 (40%) possessed a defined minimum amount of lightning activity required for further analysis. These 36 storm days were divided into two tiers according to the distribution of median daily SI values. The tier containing the 24 storm days (66.7%) with the highest median SI values possessed statistically significant lower values of 0-6 kilometer wind shear (13.8 knots) versus the 12 days in the lower tier of SI values (26.5 knots). This key environmental difference between single-cell and non-single-cell storm modes was also the most distinguishing characteristic in synoptic atmospheric composites for the two types of storm days.

Keywords: total lightning, spatiotemporal clustering, thunderstorm mode

4.1 Introduction

As discussed in Chapter 1, the importance of storm mode is readily recognized by contemporary severe weather researchers and forecasters. While detailed methodologies have been proposed for identifying the convective mode of a cell, or series of cells, by radar (e.g., Gallus et al. 2008; Smith et al. 2012a; Trapp et al. 2005), many of the characteristics associated with the storms themselves, or the atmospheric conditions that support their development, are qualitatively defined (i.e., “low shear” and “high instability” that reference the general pulse storm environment). Though common operational values exist for these thresholds (Thompson et al. 2003), cases where the observed storm mode violates the informal expectations of what a given environment would support can complicate the classification process (Csirmaz et al. 2013).

However, lightning-based classification could provide enhanced automation and objectivity to a currently labor-intensive process. This chapter provides a preliminary assessment of the viability of using spatiotemporal total lightning patterns to differentiate single-cell storms from more organized convective modes. For the purposes of this analysis, non-single-cellular storm modes will be broadly referred to as the multicell/supercell mode. While it may be argued that there exist more than two distinct storm modes, the taxonomy utilized within the study is not meant to imply otherwise; it is simply a concise method to distinguish single-cell storms from non-single-cellular modes. Although multicellular and supercellular thunderstorms are by no means equivalent modes, the spatiotemporal traits that would differentiate a single-cell storm from a multicell storm would also differentiate a single-cell storm from a supercell storm.

Thus, this preliminary study will make no attempt to discern multicell thunderstorms from supercell thunderstorms, instead combining them into one multicell/supercell category.

Following the establishment of the Geostationary Lightning Mapper (GLM) aboard the GOES-R satellite scheduled for launch in late 2015, lightning data are likely to assume more prominent roles in weather forecasting and in the research and study that underlies improved severe weather forecasting. A greater ubiquity of lightning data in the future, and the research need for stratification of storms by mode, leads to the question of whether archived lightning data can be used in research to identify storm mode.

In this preliminary analysis, the classification of storms as single-cell versus multicell/supercell storm modes during a summer season for a region of the eastern United States was predicated on the spatiotemporal distribution of total lightning detected by the ENTLN. The data analyzed in this study were gathered during the summer of 2012 over southwestern Virginia, southeastern West Virginia and northwestern North Carolina, covering an area roughly outlining the Blacksburg, Virginia, National Weather Service Forecasting Office (NWSFO) County Warning Area (CWA; Fig. 2a). The approximately 75,630 km^2 area of the study domain includes the mountainous terrain of the central Appalachians to the west and lower elevation piedmont to the east (Fig. 2b). During summer, this region of the United States is frequently characterized by warm, moist air masses that give rise to disorganized convection during the peak of daytime heating, but it is also susceptible to more dynamically-forced, organized convection associated with the mid-latitude synoptic

atmosphere. Although these more organized storm modes are most likely to occur at the beginning or end of the warm season, it is still possible for them to form at any time of year.

4.2 Data

Both ENTLN and KRNK radiosonde observations were retrieved for the period 1 May through 31 August 2012 as described in Chapter 3. This four-month window was selected based on the regional severe weather climatology compiled by the Blacksburg NWSFO which states that this time window captured 82% off all severe weather reports between 1950-2005 (Stonefield and Hudgins 2006). The ENLTN flashes analyzed were observed exclusively prior to the detection algorithm upgrade. While these data do not benefit from the improved algorithm, their use in this analysis – defining the spatial and temporal extents of total lightning clusters – will be robust to small errors in detection efficiency and classification efficiency. As noted in Chapter 3, it is possible that 0000 UTC KRNK radiosonde observations may have been influenced by convection occurring prior to the launch. However, KRNK precipitation observations obtained from the National Climatic Data Center's (NCDC) Climate Data Online (CDO) portal (www.ncdc.noaa.gov/cdo-web/) revealed that precipitation was recorded within 1.5 hours of the radiosonde launch on only 10.7% of the days considered.

4.3 Methods

a. Identification of lightning clusters

The 1,692,338 ENTLN flashes recorded between 1800 UTC and 0300 UTC (1400 and 2300 LT) each day of the period 1 May through 31 August 2012 were

isolated for further analysis. Since the major forcing mechanism for a true single-cell storm is buoyancy produced by daytime surface heating via insolation (Markowski and Richardson 2010), any flashes occurring outside of this timeframe were excluded from consideration. The summertime afternoon/evening period of the diurnal cycle represents a period during which all storm modes were possible. If a broader seasonal or diurnal range were considered, the possibility of biasing the sample towards more organized storm modes would increase. Thus, the potential differentiating capability of the lightning data source was judged to be maximized during the selected timeframe. The nine-hour temporal domain was established through consultation with forecasters at the Blacksburg NWSFO.

Flashes were organized by day of occurrence and then grouped into discrete lightning clusters using the single linkage agglomerative hierarchical clustering technique as outlined by Gong and Richman (1995). Clustering techniques, including single linkage, are a common method of analysis within the atmospheric sciences (e.g., Fovell and Fovell 1993; Kalkstein et al. 1987; Marzban et al. 2009). This specific method of clustering lightning flashes begins with each flash as a separate cluster. Clusters are then iteratively combined by merging the two clusters with the smallest calculated measure of distance separating their nearest two elements. The iterative merges continue until reaching a desired number of final clusters. The strength of the single linkage method lies in its flexibility to form clusters of unknown and often irregular shape. Additionally, this clustering procedure, along with all agglomerative hierarchical cluster techniques, is capable of classifying any number of final clusters between N (the

number of flashes in the sample) and 1. While other hierarchical clustering techniques, such as complete linkage and average linkage, also possess this trait, they did not perform as accurately on a pilot day used to test alternative clustering techniques by comparison to radar imagery.

For this analysis, the distance measure formulated for the separating distance between each flash is proportional to the magnitude of the three-dimensional vector connecting the flashes in two-dimensional space (X, Y) and time (T). The X and Y coordinates of a flash were chosen to be the Universal Transverse Mercator (UTM) easting and northing, respectively. For computation purposes the easting and northing of each flash were divided by three orders of magnitude, essentially representing the coordinates in kilometers instead of meters. For T, the original 24-hour timestamp was converted to thousands of seconds since midnight (kilo-seconds; ksec). The coordinate was then linearly scaled by a factor of 5.556 km $ksec^{-1}$ in order to standardize the relative contributions of space and time to the distance vector. This value was determined by calculating the ratio of space to time for a generic, discrete thunderstorm as defined by observations from Byers and Braham (1949) and Rauber et al. (2008) - a storm lasting one hour and attaining a 20 km cross-section at its widest (20 km/3.6 ksec = 5.556 km $ksec^{-1}$). While a 20-km diameter is large for a single-cell storm, it is an intermediate value between unorganized and organized convective modes (Rauber et al. 2008). A small cross-section might bias the clustering process to identify more “single-cell” clusters than truly exist.

No evidence of this time-space standardization could be identified in previous literature within the atmospheric sciences. However, statisticians have long debated the most appropriate method for standardizing variables across different sets of units (e.g., Everitt et al. 2001; Milligan and Cooper 1988). Consequently, standardization is a complex challenge and many different methods have been suggested. The standardization utilized in this analysis follows a modified form of standardization which performed superiorly to five other tested methods in a simulation study by Milligan and Cooper (1988). The superior form tested by Milligan and Cooper (1988) involved dividing one variable by the range of values of the other. The calculation of the 5.556 km $ksec^{-1}$ standardization factor was computed by dividing a somewhat typical range of temporal values by a somewhat typical range of spatial values. As a preliminary study, standardization was a secondary concern, and this portion of the methodology is open to refinement and improvement in future research.

To optimize computing efficiency (as the iterative nature of the clustering process makes it intensive), each day's flashes were broken into packages of approximately 4,000 flashes, with each package overlapping with the one preceding it by 5 minutes. The single linkage clustering technique was then performed on each package until only 150 distinct clusters remained. This threshold was selected since it represented a cautiously high upper limit on the number of distinct storms that might have occurred within a 4,000-flash package. Since single linkage clustering allows a single flash to constitute a cluster, in a worst-case scenario when only one distinct storm truly

occurred, it would still be apportioned 96.3% of its deserved flashes (i.e., (4,000 – 149)/4,000 = 96.3%). Days with less than 300 flashes were investigated manually.

Once again, a much deeper level of complexity belies the above methodology. The selection of the number of final clusters, 150 in this case, is a difficult and complex task that ultimately requires some element of subjectivity (Everitt et al. 2001). Since the true number of thunderstorms on a given day is unknown, it is impossible to designate the number of final clusters beforehand. Consequently, statisticians have proposed numerous methods for estimating the most appropriate number of clusters prior to analysis (Everitt et al. 2001). Thirty such procedures were evaluated by Milligan and Cooper (1985) whom documented a wide-ranging ability of the procedures to accurately ascertain the true number of clusters prior to any clustering. It should be noted then that this selection criterion holds some degree of influence over the subsequent results of the analysis. However as a preliminary study, the termination point of the clustering technique was a secondary concern within the context of this study's objective of assessing storm mode classification. This portion of the methodology is open to refinement in future research.

After all of the packages for a given day were clustered, the overlapping flashes were analyzed to identify clusters that were interrupted in the T dimension when the package was created. For instance, if during the 5 minute period of overlap, 200 flashes in package A were grouped into cluster 10A, and the same 200 flashes were grouped into cluster 48B in package B, then all flashes in cluster 48B would be added to 10A, and all the redundant flashes would be removed. At the end of the process, all unique

flashes on each day were seamlessly clustered across the entire time domain. In total, 56,697 clusters were generated for the period of consideration. This 5-minute overlap period yielded acceptable results on a series of test packages, but future studies might consider alternative overlap values.

b. Characterizing the temporal and spatial properties of the clusters

Once lightning clusters were generated for the entire 2012 convective season, each cluster was characterized in terms of beginning and end time, duration, IC flash total, CG flash total, IC+CG flash total, the maximum observed total flash rate, the time of the maximum observed total flash rate, and the average velocity of the cluster in two-dimensional (X-Y) space. The average velocity was calculated by dividing the distance between the mean center of all flashes occurring within the first minute of the cluster and mean center of all flashes occurring within the last minute of the cluster by the duration of the cluster. While one-minute mean centers appeared to satisfactorily describe storm motion, longer periods of averaging might also be considered in the future. The maximum flash rate was determined following the methodology outlined by Schultz et al. (2011). This method calculates the flash rate (flashes per minute) using the most recent two minutes of flash data. To reduce variability in the two-minute flash rate the most recent two minutes are split into two one-minute intervals and averaged together.

All clusters with beginning times prior to 1805 UTC (1405 LT) and end times after 0100 UTC (2100 LT) were excluded from further consideration. While it was previously stated that all flashes between 1805 UTC and 0300 UTC were included in the clustering

process, the temporal window was narrowed so that clusters ongoing before 1800 UTC or extending past 0100 UTC would be excluded. Artificially beginning all clusters at 1800 UTC or ending all clusters at 0100 UTC might cause truly long-lived clusters to appear misleadingly short-lived. Therefore, clusters with natural begin times after 1805 UTC and end times prior to 0100 UTC would be retained for further consideration. Figure 3 displays the results of the clustering process for a single day at the conclusion of this stage of the analysis.

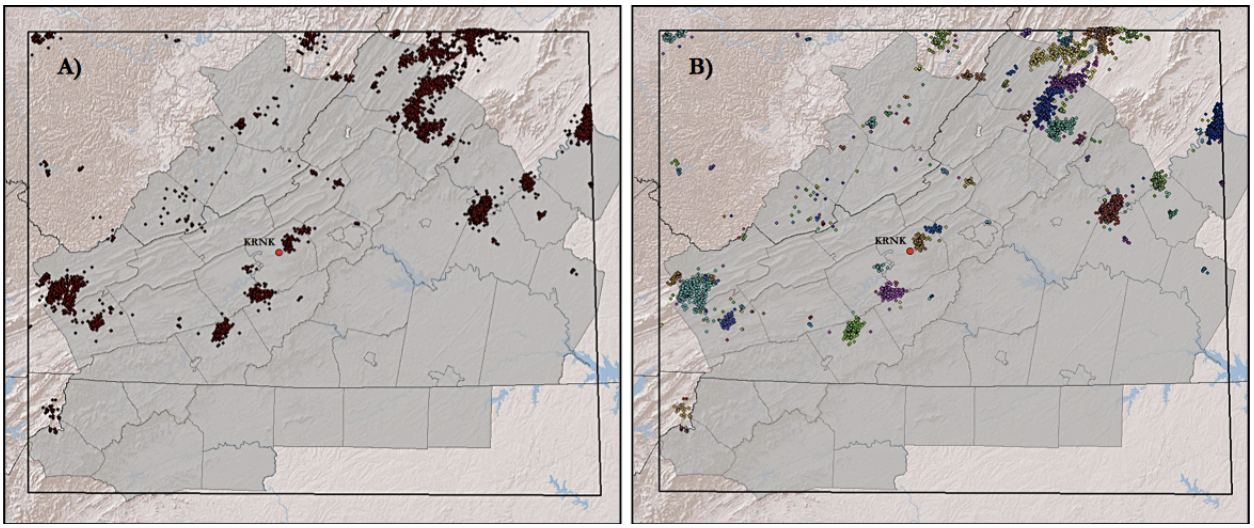

Figure 3. Lightning flashes occurring on 21 June 2012, depicted a) prior to the single linkage clustering process and b) after the results of the clustering process have been applied. Different groups are denoted by the color of the points. Thunderstorms appear as dense clumps of flashes and are easily identified via the clustering technique. The KRNK sounding site is labeled near the center of the images.

To describe the spatial characteristics of each cluster, the coordinates of all flashes representing each cluster were imported into geographic information system (GIS) software. The GIS framework presented an excellent platform to analyze the spatial properties of the clusters and has proved to be a useful analytical tool in recent total lightning studies (Rudlosky and Fuelberg 2013). The “Minimum Bounding Geometry” (MBG) tool within the Environmental Sciences Research Institute’s (ESRI)

ArcMap version 10.0 was used on each cluster to draw the convex hull bounding polygon of (1) all flashes that occurred during the cluster's 5 minutes of peak lighting activity (Fig. 4), from here on referred to as the "max flash rate polygon," and (2) all flashes occurring across the entire lifetime of the cluster, from here on referred to as the "total lifetime polygon". The MBG tool was also used to draw the circumscribing circle of each max flash rate polygon (Fig. 4), and its diameter was recorded for later use. The area of the max flash rate polygon was determined using ArcMap's "Calculate Geometry" tool and recorded alongside the attributes described above. Since the calculation of a cluster's areal extent was foundational to this stage of the analysis, all clusters with fewer than three flashes were discarded. By definition, these clusters did not possess a calculable area, and therefore could not be analyzed spatially.

The total lifetime polygon was also used to eliminate any clusters that occurred within 2 km of the domain boundary. If only partial lightning data for a cluster existed due to the restriction of the study domain, a large, long-lived cluster might appear small and brief. The 2-km buffer ensured that such clusters were eliminated from further consideration. Unfortunately, in a few instances, this buffering process removed very long-lived clusters that stretched across much of the study area. While eliminating these clusters was undesirable, it was judged to be better to exclude them than allow incomplete clusters to remain in the analysis. After removing all clusters beginning before 1805 UTC (1405 LT), ending after 0100 UTC (2100 LT), possessing fewer than three flashes, or existing within 2 km of the domain boundary, 8,445 clusters remained for further analysis.

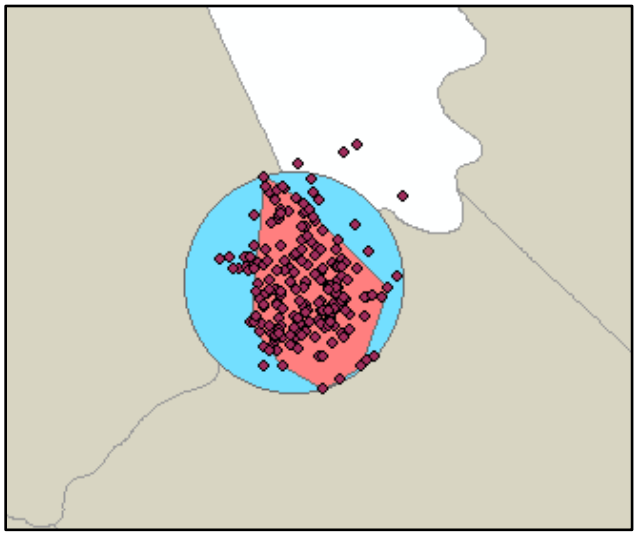

Figure 4. Example minimum bounding geometry as applied to a single lightning cluster. The individual dots represent all the flashes that were grouped within the cluster while the irregular polygon in dark gray represents the max flash rate polygon. The light gray circle is the circumscribing circle used to calculate the compactness measure.

The final descriptive quantity generated for each cluster was a measure of "compactness" derived from the diameter of the circumscribing circle and the area of the max flash rate polygon. The calculation of compactness follows the formula summarized by Maceachren (1985), whereby the diameter of the circle with an area equivalent to the max flash rate polygon is divided by the diameter of the circumscribing circle. For a very circular polygon, the diameter of the equivalent circle and the circumscribing circle will be very similar, yielding a compactness value near one. Oppositely, very linear shapes will have much larger circumscribing diameters, and thus, compactness scores closer to zero. This measure is an advantageous descriptor of the clusters since more circular clusters are distinguished from more linear clusters. Since a linear storm structure is often indicative of increased storm organization, and possibly a non-single-cell mode, it is important to describe this spatial attribute of each cluster.

c. Quantifying Thunderstorm Organization

With a full suite of spatial and temporal attributes calculated for lightning clusters that occurred entirely within the bounding domain, the objective then shifted towards assigning each cluster a score representing its duration, areal extent, average velocity and shape. To aid in this assessment, a "storm index" (SI) was developed to measure how well the duration, areal extent, shape and motion of a cluster matched the scientific and operational knowledge of single-cell storm behavior. The goal of the SI was to assign high scores to small, non-linear, short-lived and slow-moving clusters while assigning low scores to large, asymmetric, long-lived, and fast-moving clusters. Storms adhering to the former expectations would be considered single-cells while storms possessing the latter attributes would be considered multicell/supercell.

It has previously been hypothesized that convective mode is a continuous spectrum with no clear boundary between modes (Weisman and Klemp 1982, 1984). Therefore, it is necessary that the SI be a flexible measure that compares a storm's overall behavior to single-cell expectations, but without using a hard cut-off for any single parameter. Since single cell thunderstorms are the least organized form of convection, these storms served as the baseline by which more organized modes would be assessed. Therefore, for each parameter used to characterize a cluster/storm, two values were selected: one typical of a single-cell thunderstorm (where any storm meeting this mark could be safely considered single-cellular in regard to the selected parameter) and one typical of a non-single-cell thunderstorm (where any storm violating this mark could be safely considered non-single-cellular in regard to the selected parameter). Any storm meeting the single-cell ordinary storm threshold would receive a

one for the selected parameter. The score would then linearly decay to zero, with the zero value represented by the non-single-cell storm threshold. However, scores generated by this method were not restricted to between 0 and 1 (Fig. 5). Instead they were allowed to decay past zero so that storms with attributes grossly violating a parameter could be appropriately qualified. As a preliminary study, this analysis assumed a linear decay function between the two thresholds; however, it is possible that other decay models might be more appropriate or yield stronger results.

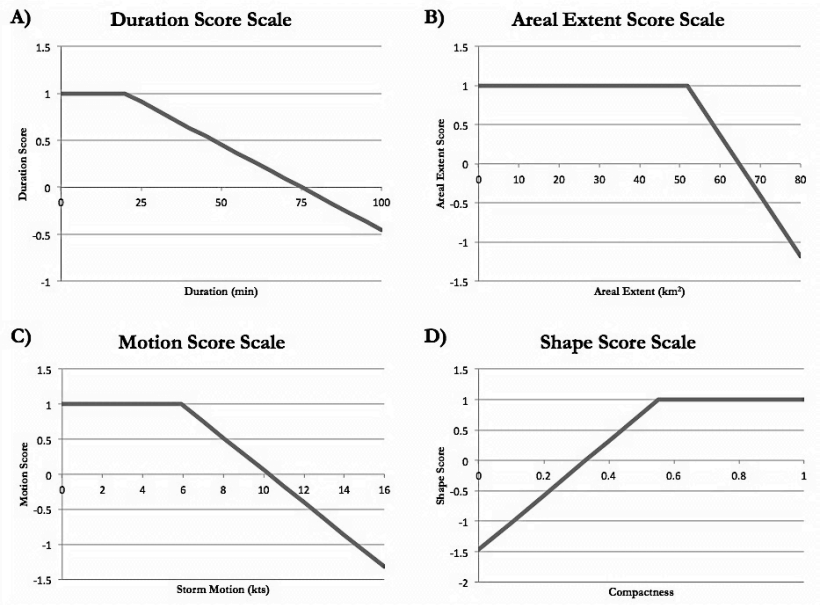

Figure 5. Standardization functions for the four storm parameters included in the SI – a) duration, b) areal extent, c) storm motion and d) shape. While the graphs imply there is a lower cut-off, duration, motion, and areal extent scores have no lower limit.

Unfortunately, there is very little literature to guide the threshold definitions for the different structural characteristics of ordinary and non-ordinary thunderstorms. The primary source utilized is the 1949 *Thunderstorm Project* sponsored by the U.S. Weather Bureau (Byers and Braham 1949), and it was the range of observations in this published study that provided the thresholds for duration, area and motion used in this work. The study's focus on comprehensively documenting nearly every spatial and

temporal attribute of short-lived, single-cell thunderstorms qualifies it as an excellent resource despite being conducted over 60 years ago.

i. Duration thresholds

According to the observations of Byers and Braham (1949), isolated cell thunderstorms produced very short-lived radar echoes, lasting only 20 minutes on average. In order to place a conservative lower limit on the total duration of a single-cell storm, 20 minutes was selected as the lower threshold for the duration score. Any cluster lasting less than 20 minutes was safely within the limits of the single-cell storm regime. Additionally, the observations of the report placed the maximum combined duration of all three ordinary thunderstorm stages (cumulus, mature and dissipating) at 75 minutes (Byers and Braham 1949). This duration was selected as the upper threshold for the single-cell regime meaning any storm lasting longer than 75 minutes would receive a duration score less than zero. The function relating storm duration to the numerical score assigned to storm duration is depicted in Figure 5a.

ii. Areal extent thresholds

Within *The Thunderstorm Project*'s discussion of the horizontal extent of thunderstorms, it is shown that an areal extent of 51.8 square kilometers was the average for storms with cloud tops greater than 25,000 feet (7,620 m) (Byers and Braham 1949). Since both older and more recent studies (Shackford 1960; Zhang et al. 2013) have found the 20,000 – 30,000-foot (6,096 – 9,144 m) cloud top range to be the minimum for steady lightning production, 51.8 square kilometers was selected to represent the lower threshold. While Byers and Braham (1949) did not include the

individual observations, presenting group averages instead, the figures included in the report show that a cross-sectional area of 64.7 square kilometers represents roughly the 85th percentile for observed thunderstorms. This value was selected as the upper areal extent threshold, rather than the largest observed storm, since it is more likely storms nearer the maximum areal extent might be aided by undesired atmospheric organization. The function relating the areal extent of a storm to the assigned score based on areal extent is depicted in Figure 5b.

iii. Motion thresholds

The lower threshold on storm motion was set equal to the lowest mean storm motion observed within the *Thunderstorm Project* (Byers and Braham 1949) through the study's data collection effort in Florida (5.9 knots, 3.0 m s^{-1}). Similarly, the upper threshold (10.3 knots, 5.3 m s^{-1}) was set equal to the largest mean storm motion observed in the data collection in Florida. Mean storm motions less than 5.9 knots were considered safely within the single-cell regime, while storm motions greater than 10.3 knots were deemed less likely to be characteristic of the single-cell mode. Although storm motion measurements were collected in both Florida and Ohio as part of the *Thunderstorm Project*, the values from Florida were selected for use here since it was more likely that these storms were embedded within a weakly-sheared air mass. The function relating storm motion to the score assigned to storm motion is depicted in Figure 5c.

It should be noted that supercell thunderstorms have been observed to remain nearly stationary while still maintaining supercellular characteristics (Bunkers et al.

2000). In cases such as these, a highly organized storm mode would be mistakenly scored as a single-cell with respect to the storm motion threshold.

iv. Shape thresholds

While Byers and Braham (1949) documented the shape of storms in a handful of cases, the observations were not great enough in quantity or detail to aid in the determination of the shape threshold. Therefore, the thresholds for uniformity in the shape of the lightning patterns were extracted from the total distribution of the compactness measure, the calculation of which was outlined earlier. However, the histogram of compactness values for the 8,445 remaining clusters is bimodal with a clear maximum at compactness measures below 0.10 (Fig. 6a). As illustrated in Figures 6b and 6c, this is a result of the large number of few-flash clusters possessing very low compactness values. Clusters with very few flashes will likely appear irregular and result in a large number of very low compactness scores.

Consequently, the upper and lower quartiles of the distribution are heavily influenced by these numerous, few-flash clusters that likely do not represent legitimate convective events. In order to prevent shape scores from being heavily influenced by what is quite possibly noise in the data, the distribution used to determine the 25^{th} and 75^{th} percentile of compactness measures ignored all clusters with fewer than ten flashes. Figure 6d depicts the distribution of compactness measures once clusters with fewer than ten flashes are excluded. These clusters were not discarded; they were simply excluded from the distribution while establishing the shape thresholds. The lower threshold for shape was selected as the 75^{th} percentile representing the top quartile of

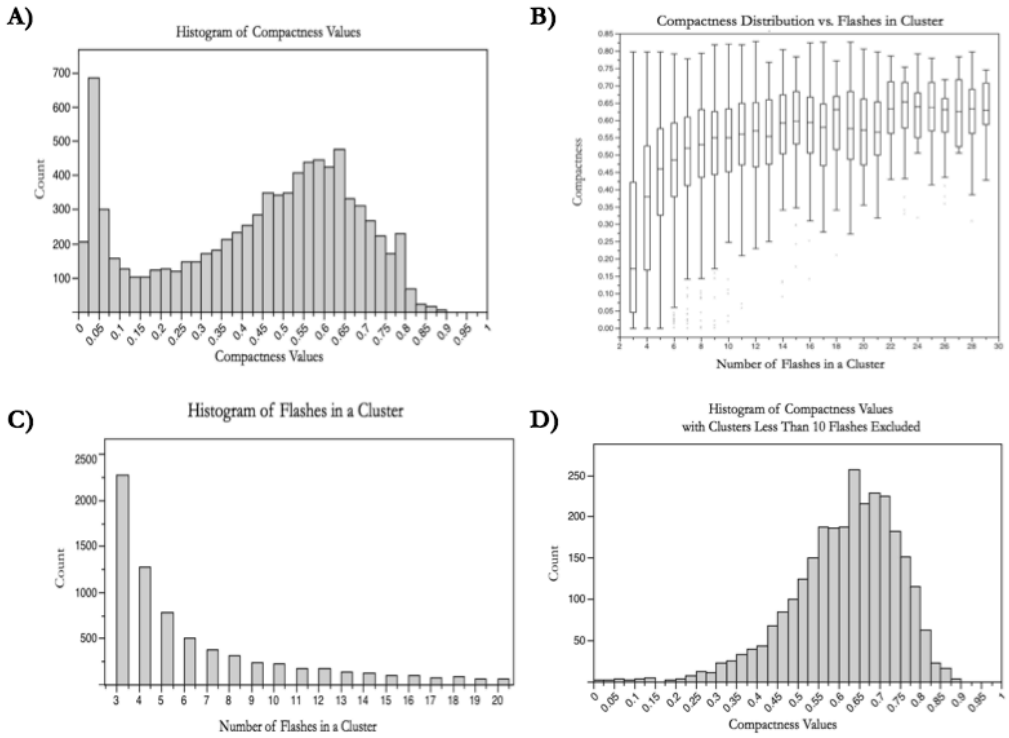

Figure 6. Histograms depicting the distribution of a) compactness values from all 8,445 clusters with three or more flashes, b) a series of box plots illustrating the distribution of compactness values for all clusters with a given flash total, c) number of clusters with flash totals between 3 and 20 total flashes, and d) compactness values from all 2,748 clusters with ten or more flashes.

uniform clusters. Alternately, the 25th percentile was selected as the upper limit representing the lowest quartile of circularity measures. The function relating storm compactness to the score used to represent storm shape is depicted in Figure 5d.

The thresholds selected for each cluster attribute are, of course, subjective, and arguments could be made for other threshold values. As such, several different threshold values were utilized prior to finalizing those defined above, and the results remained rather consistent. Under any selection of thresholds, small, short-lived, slow-moving, circular clusters of lightning flashes receive higher scores and large, long-lived, fast-moving, asymmetrical clusters of flashes receive lower scores.

v. Relative parameter weights

With scores for each parameter established, the individual scores needed to be combined into a single SI score. Since the SI is intended to be a simple linear combination of the scaled parameters, only the relative weights of the parameters were needed to calculate the SI. With no published work available to guide this task, NWS operational forecasters from the Blacksburg NWSFO were engaged to gain forecaster perspectives. While the forecasters had little experience with interpreting total lightning data, they were asked to compare the relative importance of each storm parameter as they would interpret them using radar imagery. Since the index is only concerned with the relative importance of each parameter, it was not necessary for the forecasters to be familiar with the lightning data source.

The forecaster perspectives were quantified using the Analytical Hierarchy Process (AHP) as described by Wind and Saaty (1980). Each forecaster was asked to make pairwise comparisons between each unique combination of the four chosen parameters, and for each pairing, choose which parameter was more important in discerning a/an single-cell/ordinary thunderstorm mode. A rating scale from 1-9 was then used to describe the degree to which the more important factor was considered to be superior in the forecaster's view. A rating of 1 meant that the "two activities contribute equally to the objective" while a rating of 9 meant that "the evidence favoring one activity over the other is the highest possible order of affirmation" (Wind and Saaty 1980). Individual hierarchies were established for each of the five forecasters from the Blacksburg, Virginia, NWSFO who provided input to the local Science and Operations Officer (SOO) before calculating the geometric means of the individual results to

produce a group decision (Saaty 1994). Freely available software from Business Performance Management (http://bpmsg.com/) was used to perform the AHP. The geometric mean of the five results yielded the following group result: Duration – 20.3%, Motion – 18.0%, Area – 17.4%, Shape – 44.3% (Stephen Keighton, SOO, NWSFO Blacksburg, personal communication, 2013). With a consistency ratio of 0.4%, the forecaster responses were excellent candidates for the AHP.

With relative weights established, the SI was calculated for each storm using the formula shown below. The terms within the expression are written in conditional notation in order to communicate the piece-wise nature of the functions shown in Figure 5. If the given parameter satisfies the condition listed first within the parenthesis, then it receives a score of one for that parameter score. Otherwise, the final expression within the parenthesis applies.

$$SI = IF(AREA \le 51.8,1,(64.7 - AREA)/12.9) \times 17.4$$
$$+IF(COMPACTNESS \le 0.55,1,(COMPACTNESS - 0.33)/0.22) \times 44.3$$
$$+IF(DURATION \le 20,1,(75 - DURATION)/55) \times 20.3$$
$$+IF(MOTION \le 5.9,1,(10.3 - MOTION)/4.4) \times 18.0$$

vi. Filtering Misleading Clusters

Although clusters of one and two flashes were discarded during the spatial analysis stage, further refinement was required to determine the minimum flash threshold at which a cluster's SI score represented a meaningful commentary on its parent environment. For the parameters utilized within the SI to have a practical meaning, a minimum cluster flash threshold is needed. For example, it is difficult for a few-flash cluster to be anything but small, short-lived and display little mean movement. As such, small clusters will inevitably possess high SI scores regardless of the

convective environment in which they formed. Oppositely, many-flash clusters can easily be either long-lived or short-lived, large or small, stationary or mobile, and circular or linear.

To establish the minimum flash threshold, the SI was compared to the condition of the atmosphere in which each cluster formed. Traditional definitions assert that single-cell thunderstorms form in environments with weak vertical wind shear (Markowski and Richardson 2010). Thus, the median SI on a given day should be inversely proportional to the vertical wind shear. Median daily SI versus wind shear was chosen over individual cluster SI versus wind shear so that the relationship would not be skewed by single days with many clusters. The minimum cluster flash total required for a cluster to be included in the analysis was varied between three and 300 flashes at one-flash intervals. In each case, the Pearson correlation coefficient was calculated between mean daily SI and 0-6 km wind shear as measured from the 0000 UTC KRNK sounding. The results indicate a very clear step in correlation coefficients near a per cluster minimum flash threshold of 50 (Fig. 7). Thus, a minimum threshold of 50 flashes was selected to differentiate between misleading clusters of lightning flashes and clusters that reasonably reflected the organization of their host environment.

d. Individual Thunderstorm and Thunderstorm Day Identification

With a preliminary minimum cluster flash threshold established, it was still necessary to identify the minimum cluster size that would best characterize a healthy, legitimate thunderstorm. While a 50-flash minimum seemed to eliminate a misleading subset of few-flash clusters with high SI scores, it cannot yet be said whether all of the

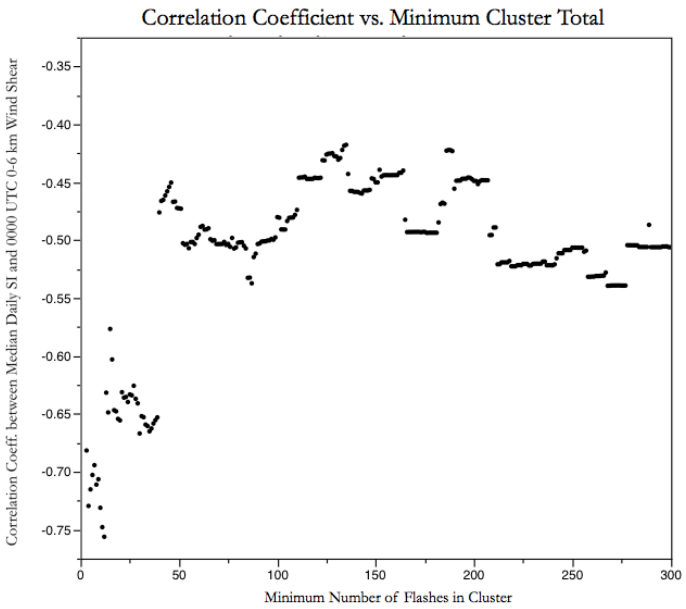

Figure 7. Scatterplot illustrating the Pearson correlation (R) coefficient between the median daily SI and 0-6 km 0000 UTC wind shear as a function of the minimum flash total in a cluster. Above 50 minimum flashes, the relationship is relatively consistent.

remaining clusters represent informative convective events. As a preliminary study, this analysis chose to rely upon the SI scores of clearly established, healthy convection as the most dependable indicators of the parent convective environment. Thus, an additional threshold was selected to identify the minimum cluster flash total that would best characterize the state of the atmosphere in which the cluster formed. Future studies might consider an enhanced methodology that avoids the institution of a second minimum cluster flash threshold.

Since storm mode is largely dependent on the local wind field (Markowski and Richardson 2010), the state of the atmosphere in which the storms formed was used to calibrate the results of the SI. Additionally, yet to be determined was the number of individual clusters per day necessary to yield a robust description of the convective environment. For instance, it would likely be inaccurate to use the data for the regional

atmospheric sounding (KRNK; Fig. 2) to characterize the environment as conducive to single-cell or multicell/supercell thunderstorms on a day marked by a single cluster of 50 flashes located far from the sounding site (KRNK; Fig. 2). To establish a number of daily discrete clusters necessary to provide robustness in atmospheric analyses, daily cluster minimums were instituted and the correlation between the median daily SI and 0000 UTC wind shear was recalculated while excluding days failing to meet each cluster minimum that was tested. However, instituting the daily minimums also decreased the sample sizes used to generate the correlation coefficients, and thus, the value of the coefficient became increasingly sensitive to individual data points. In order to conserve sample size and the reliability of the correlation calculation, five series of correlations were calculated (Fig. 8) – one each for minimum daily number of clusters of 1, 2, 4, 6, and 8.

Between 50-100 flashes, two of the five series (6 and 8 minimum daily clusters), demonstrate a strengthening correlation between median daily SI and 0000 UTC 0-6 km shear. These two series both reach a maximum inverse correlation near 90 flashes with the correlation coefficient stabilizing near 100 flashes, indicating that clusters with at least this number of flashes most accurately and consistently characterize environmental wind shear. Since only two data series possess a stable minimum correlation near 100 flashes, it seems that the most accurate characterization of the convective atmosphere can be achieved using either a 100-flash, 6-cluster minimum threshold or a 100-flash, 8-cluster minimum threshold. Since the SI-shear correlation when using the 6-cluster minimum is more consistent across the entire minimum flash

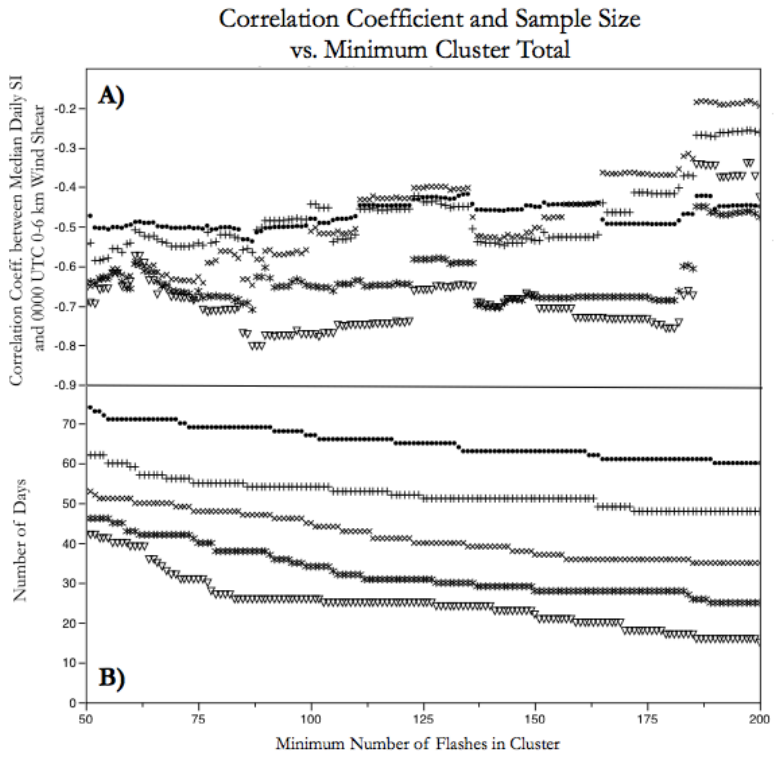

Figure 8. (a) Same as Figure 7 with five series illustrated, each representing the Pearson correlation (R) coefficient for the following daily cluster minimums: 1 (□), 2 (+), 4 (×), 6 (∗), and 8 (∇). Also included (b), are the number days used to calculate R at each minimum cluster flash total.

domain, the 100-flash and 6-cluster daily minimums were instituted for the remainder of the analysis. This minimum cluster total agrees well with the observations of Goodman et al. (1988) whom documented a robust, 116-total-lightning-flash thunderstorm within a weakly-sheared environment. From here on, clusters with at least 100 flashes will be referred to as “lightning-defined (LD) storms,” and days with at least six LD storms will be referred to as “storm days”. While it is possible that the 0000 UTC (2000 LT) soundings were influenced by convection occurring earlier, wind shear measured at that time exhibits a stronger correlation to median daily SI than does wind shear at 1200 UTC (0800 LT) (Fig. 9), and therefore it was used as the standard to which the SI was

compared and 0000 UTC variables were chosen to characterize a day's convective environment.

4.4 Results and Discussion

In this section, the LD storms and storm days determined using the previously defined process are compared to the environments in which they formed. Days documenting predominantly LD single-cell storms are compared against the traditional expectations of a single-cell storm environment while days with

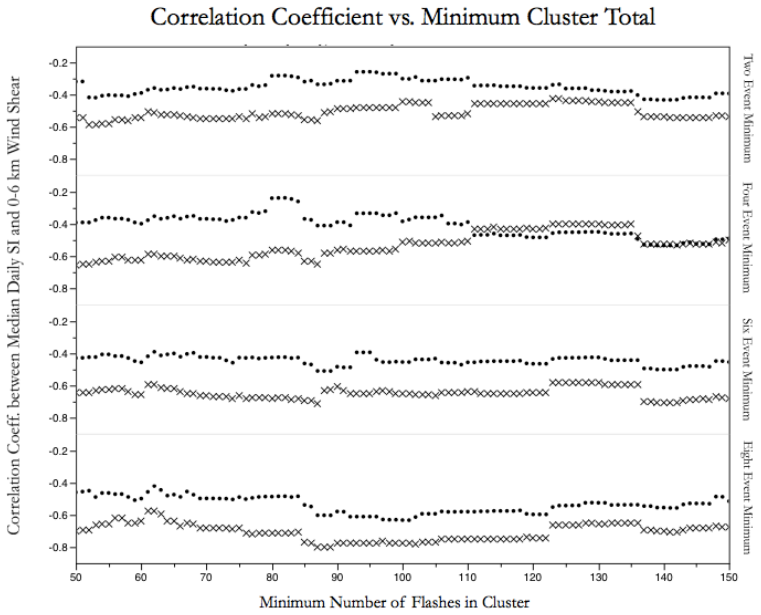

Figure 9. Scatterplots illustrating the correlation of median daily SI to 0000 UTC 0-6 km wind shear (×) and 1200 UTC 0-6 km wind shear (*) as a function of cluster minimum flash total. Each series represents a different daily LD storm minimum for consideration. Evident is that 0000 UTC wind shear displays a stronger correlation with SI.

predominantly LD multicell/supercell storms are compared against the traditional expectations of an organized storm environment. In some respects, this section serves as a validation of the above method.

a. Analyzing the SI distribution

Of the 123 days between 1 May and 31 August 2012, lightning was observed within the study area on 97 days. However, three lightning days recorded all flashes outside of the 1805-0100 UTC temporal bounds, and 23 days did not produce a cluster with at least 100 flashes. Of the 71 days with at least one 100-flash cluster, 35 days did not contain at least six such LD storm. The result was a final pool of 36 thunderstorm days. The histogram (Fig. 10) of the median daily SIs was used to subjectively group the 36 days into two classes (Table 1) based on the distribution of the scores. The use of

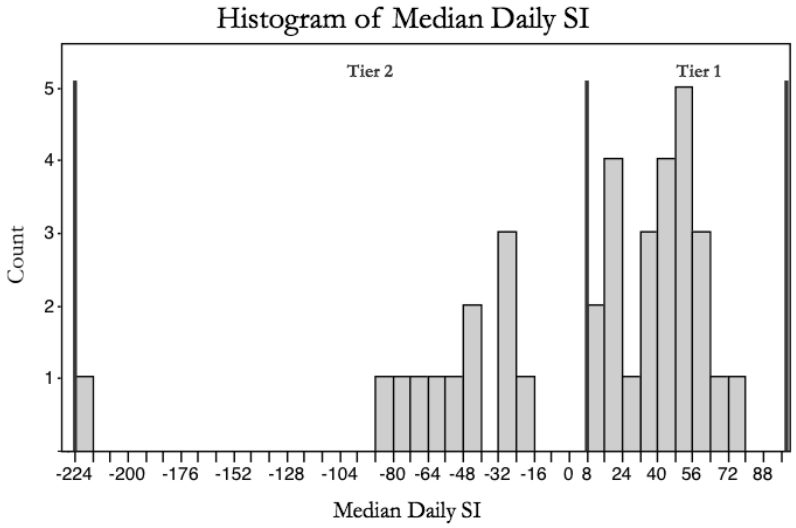

Figure 10. Histogram representing the distribution of median daily SI scores. The histogram was divided into two tiers (black lines) for further analysis.

Tier	Lower Limit	Upper Limit	Days
1	8	100	24
2	-224	8	12

Table 1. The upper and lower median SI limits used to define each tier as well as the number of days captured within the thresholds. Values are unit-less SI scores.

median daily SI tiers allows for a comparison between days on which the simple majority of storms were quantified as single-cells and days on which the majority of storms were quantified as multicells/supercells. Since storm mode is largely a function

of the parent atmosphere, 0000 UTC 0-6 km wind shear should be lower on predominantly LD single-cell days in order to remain consistent with traditional definitions. Thus, summary statistics for each tier were generated to characterize the atmosphere for the group of days in each tier (Table 2).

A pooled *t*-test for unequal variance was conducted (also referred to as a Welch's analysis of variance procedure) to test the differences in the distributions of 0000 UTC 0-6 km wind shear for statistical significance. This test yielded a p-value of 0.0102 suggesting that 0000 UTC 0-6 km wind shear on Tier 1 days is statistically lower than on Tier 2 days with nearly 99% confidence. Based on these results, Tier 1 is consistent with the expectations of a weakly-sheared single-cell thunderstorm environment while Tier 2 matches the characteristics for a more strongly sheared multicell/supercell environment. Though the mean shear on Tier 2 days (26.5 kts, 13.6 m s^{-1}; Table 2) is much weaker than values typically associated with supercell thunderstorm environments (Thompson et al. 2003), the values satisfactorily correspond to wind shear values supportive of multicell storms (Markowski and Richardson 2010). Since it is likely that organized storms occurring during the 1 May – 31 August time period in this region were predominantly multicellular as opposed to supercellular, a mean shear of 26.5 kts is a reasonable characterization for the multicell/supercell category.

It is worth noting that several of the Tier 2 days recorded very low 0-6 km wind shear values (<10 kts, 5.1 m s^{-1}). While traditionally, these days might have been characterized as single-cell environments, comparison to radar revealed that these storms were closely tied to the heterogeneous topography of the study area. The highly

Tier	Mean 0000 UTC 0-6 km Shear ± Standard Error (kts)
1	13.8 ± 1.8
2	26.5 ± 2.6

Table 2. Mean 0000 UTC 0-6 km wind shear (knots) plus/minus standard error of the mean (knots).

variable terrain of the study domain frequently leads to preferential storm propagation along differential heating boundaries associated with ridgelines [J. Hudgins, Lead Forecaster, NWSFO Blacksburg, 2013, personal communication]. The resulting lightning clusters consequently appear larger and more linear than anticipated. This topographic influence on storm propagation has been well-documented in mountainous terrain (e.g., Hallenbeck 1922; Klitch et al. 1985).

Additionally, four Tier 1 days recorded 0-6 km shear greater than 20 kts (10.3 m s^{-1}) with the highest observation being 24.9 kts (12.8 m s^{-1}). While still at the low end of the range of common shear values associated with organized, multicellular/supercellular storm modes (Markowski and Richardson 2010), these values might be somewhat higher than operationally expected for a single-cell thunderstorm day. However, as their high SI scores indicate, the median LD storm on these days was nonetheless a relatively small, short-lived thunderstorm for which the spatial and temporal properties were indicative of a single-cell mode.

As previously stated, a potential advantage of lightning-based classification is the ability to automate a traditionally labor intensive task that relies on radar analysis. As such, no effort was made in this preliminary study to individually classify all 470 LD

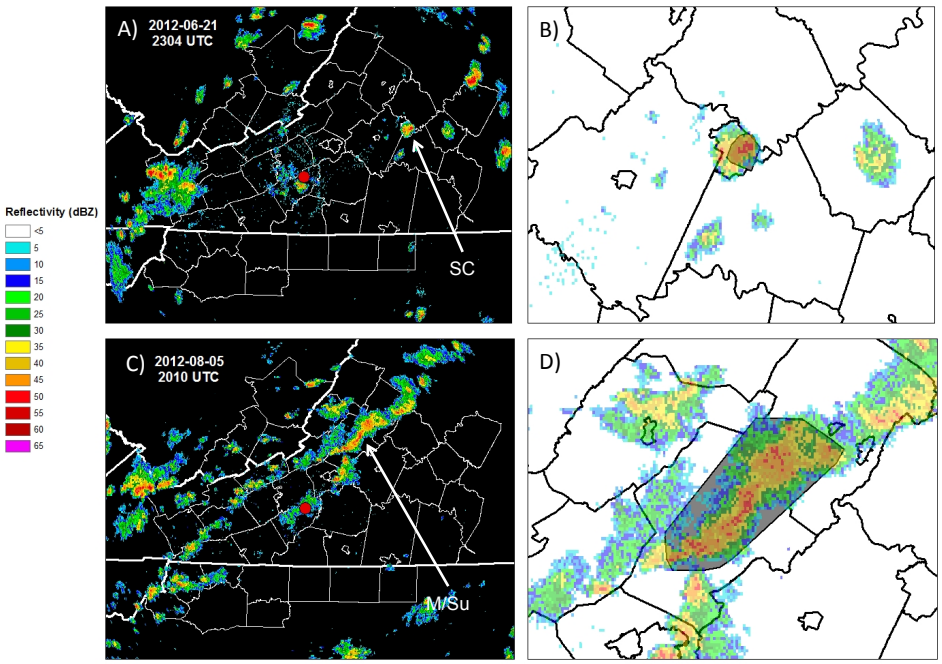

Figure 11. Comparison of the SI results to radar imagery. Panels (a) and (b) illustrate a LD single cell thunderstorm (labeled "SC") with an SI score of 80. Panels (c) and (d) depict a LD multicell/supercell (labeled "M/Su") with an SI score of -1205. The transparent gray polygons in (b) and (d) represent the minimum bounding polygon for the five minutes of peak lightning activity used to calculate the areal extent scores. The KFCX WSR-88D radar site is depicted by a red dot at the center of (a) and (c).

single-cell and multicell/supercell storms as guided by existing radar-based classification techniques (e.g., Smith et al. 2012). However, each single-cell day and multicell/supercell day was compared against radar to ensure they met the subjective operational expectations of their respective radar structure. As an example, Figure 11 contains a comparison of two thunderstorms, one LD single-cell and one LD multicell, against KFCX WSR-88D radar imagery with the max flash rate polygons overlaid.

b. Synoptic atmospheric evaluation of SI categories

The stratification of thunderstorm days also allows for an evaluation of how the mean synoptic patterns for the LD storm modes compare to traditional expectations for single-cell and multicell/supercell convective environments. For each category of storm

days, daily mean composites of the synoptic-scale atmosphere were generated to illustrate the synoptic meteorological characteristics of days on which predominantly LD single-cell or predominantly LD multicell/supercell thunderstorms occurred. The publicly available Earth Systems Research Laboratory (ESRL) Physical Science Subdivision (PSD) Daily Mean Composite tool (www.esrl.noaa.gov/psd/data/composites/day/) for depicting re-analysis data (Kalnay et al. 1996) was used to generate the maps. It should be noted that LD single-cell and multicell/supercell days were both evenly distributed throughout the 1 May – 31 August time period, minimizing the influence of seasonal variation in the composite synoptic patterns.

Synoptic maps of 500 hPa and 850 hPa geopotential heights (Figure 12) illustrate greater values indicative of a warmer lower atmosphere across the eastern United States on single-cell days compared to multicell/supercell days. A westward expansion of the eastern Atlantic Ocean “Bermuda High” is evident at 850 hPa on LD single-cell days (Fig. 12b) relative to LD multicell/supercell days (Fig. 12c). This circulation feature has been long tied to eastern United States summer precipitation patterns (Stahle and Cleaveland 1992). During LD multicell/supercell days, a trough in the 850 hPa height pattern is evident in the Great Lakes region (Fig. 12c). This is in contrast to the pattern on LD single-cell days (Fig. 12d) and suggests a more dynamic atmosphere that could yield the mechanical forcing for sustaining larger and longer-lived storms on LD multicell/supercell days.

While it might be expected that moisture and instability would not differ greatly between single-cell and multicell/supercell days (Fig. 13), the link between storm mode

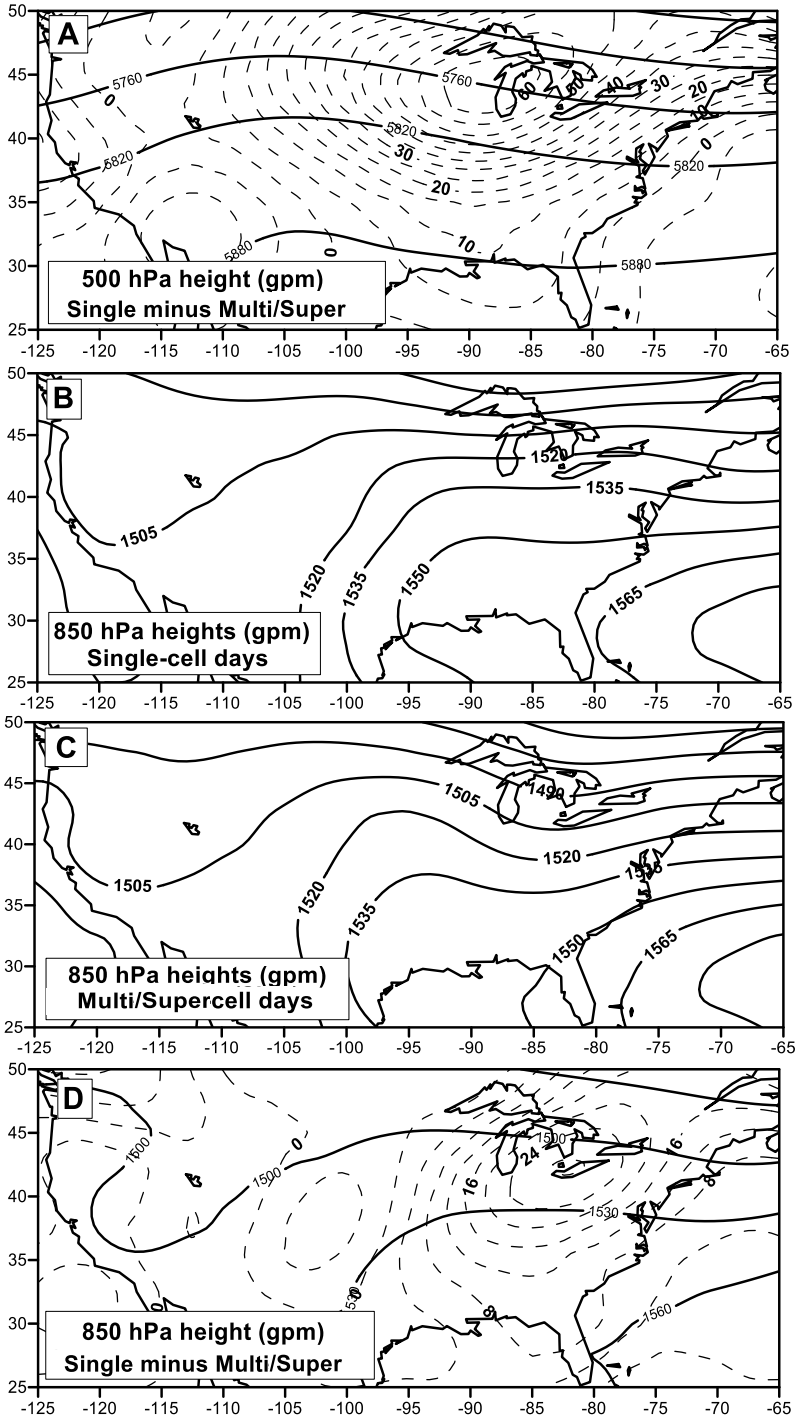

Figure 12. Composite synoptic maps for LD single-cell and LD multicell/supercell days. In (a), the geopotential height of the 500 hPa level on LD multicell/supercell days is subtracted from the equivalent value of LD single-cell days (dotted lines) with 30-year climatological normal values overlaid (solid lines). Additionally, the geopotential height of the 850 hPa level for LD single-cell days only (b) and LD multicell/supercell days only (c) are shown. Map (d) is identical to map (a) except calculated for the 850 hPa pressure level.

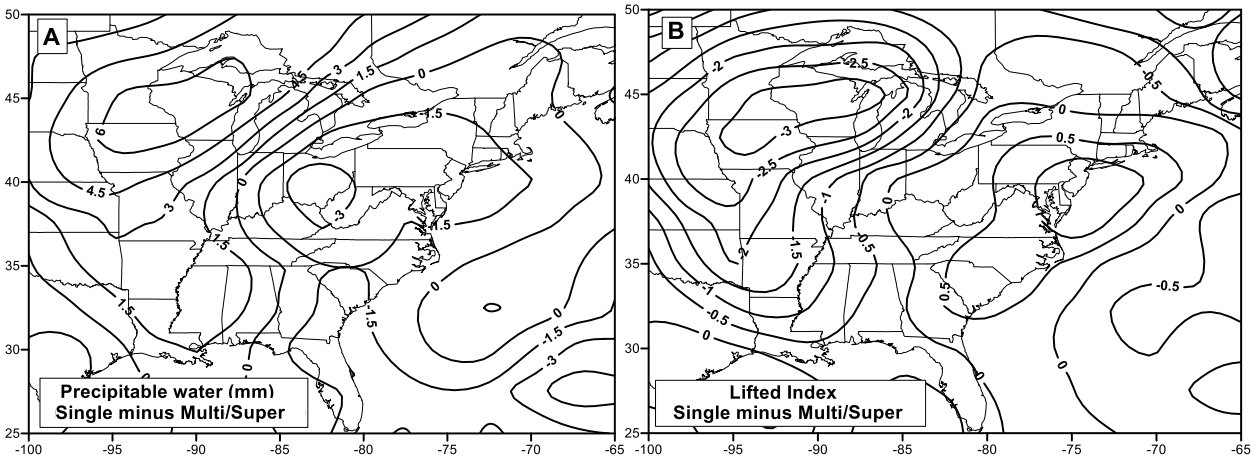

Figure 13. A comparison of precipitable water values (a) and lifted indices (b) on LD single-cell and LD multicell/supercell days. For each figure, the respective value on LD multicell/supercell days were subtracted from the equivalent value for LD single-cell days.

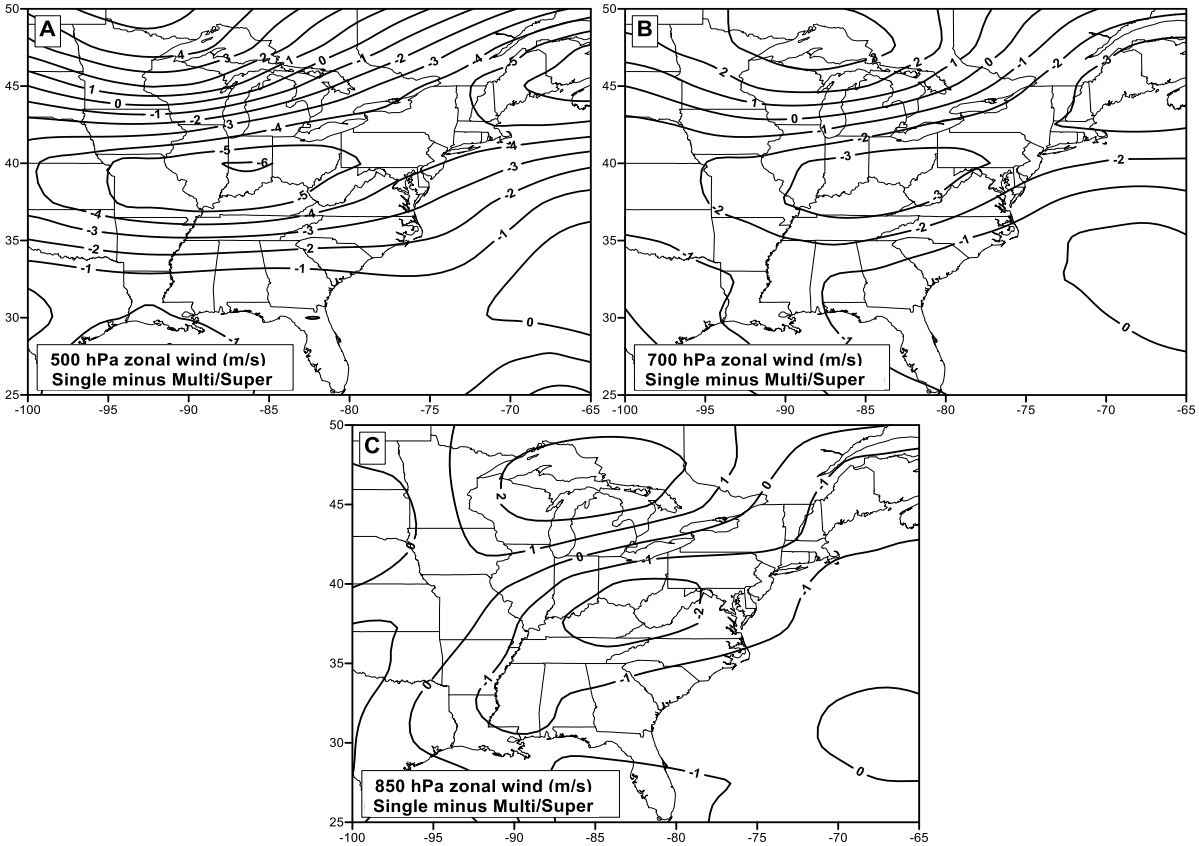

Figure 14. A comparison of zonal wind values at the 500 hPa (a), 700 hPa (b), and 850 hPa pressure levels on LD single-cell and LD multicell/supercell days. For each figure, the respective value on LD multicell/supercell days were subtracted from the equivalent value for LD single-cell days.

and atmospheric wind shear leads to an expectation of differences in the strength of atmospheric flow in the mid- and low-levels of the atmosphere on the two types of days. This appears to be the case when examining composites of zonal wind through the depth of the lower atmosphere (Fig. 14). Although zonal wind only captures the east-west component of the wind velocity, it was judged that this quantity would highlight any basic differences in the magnitude of the synoptic wind field. If differences in the combined *u* and *v* components of the vector wind were shown, the magnitude of the difference vector would always be positive and it would be unclear which set of days experienced a stronger wind field. Vector wind maps were generated for each set of days to confirm the presence of primarily east-west geostrophic flow, ensuring meaningful representation of the difference in zonal wind between the two sets of days.

The large swath of negative values at the 500 hPa (Fig. 14a), 700 hPa (Fig. 14b), and 850 hPa (Fig. 14c) pressure level indicates that winds were indeed stronger on LD multicell/supercell days than single-cell days. The stronger wind fields depicted in Figure 14 would likely contribute to the higher 0-6 km wind shear values observed on LD multicell/supercell days. When combined with the results shown in Figures 12 and 13, it is apparent that LD multicell/supercell days are potentially characterized by the approach of upper level dynamical support that is not present during LD single-cell days. The relative similarity of precipitable water and lifted index values characterizing LD single-cell and multicell/supercell days suggest that LD multicell/supercell storm days occur in the warm, moist air mass ahead of a possible surface front. This would support the greater 500 hPa and 850 hPa geopotential height differences located well

northwest of the study area. Observations in these areas would reflect conditions west of the front, typically cooler (Fig. 12a, 12c), less humid (Fig. 13a), and more stable (Fig. 13b) than ahead of it.

Taken in their entirety, the synoptic composites indicate that humidity and instability are comparable between LD single-cell and multicell/supercell days across the study area. However, wind strength and 850 hPa geopotential height patterns (Fig. 12c) suggest that LD multicell/supercell days are more dynamically driven than single-cell days. These synoptic differences are supported by previous research findings. Fuelberg and Biggar (1994) observed very similar thermodynamic regimes between days with “strong convection” and “weak convection” while thermodynamic variables between days with convection versus without convection yielded statistically significant differences.

4.5 Conclusions

This chapter represents a preliminary attempt to classify thunderstorms into two basic categories of storm mode using the spatiotemporal distribution of total lightning clusters. The results presented here suggest that spatiotemporal total lightning patterns can be used to differentiate between single-cellular and more organized storm modes. Days exhibiting a majority of smaller, shorter-lived, slower-moving and more circular storms were characterized by significantly weaker shear than days with a majority of larger, longer-lived, faster-moving and more linear storms according to the statistical assessments. As total lightning data continue to gain prominence within the operational

forecasting toolset, the integration of lightning data into traditional storm classification research methodologies could prove a fruitful addition.

Though radar-based classification possesses a much stronger pedigree than lightning-based classification, the potential benefit of this new classification tool is very attractive. LD storms can be easily analyzed for “total lightning jumps” (Schultz et al. 2009, 2011), a recent focal point of severe weather research. Additionally, a standard definition of LD storm modes could allow for the frequency and intensity of thunderstorms to be relatively easily tracked through time – helping clarify potential implications of climate change.

Many aspects of the analysis are open to refinement and improvement by future researchers. Most notably: the choice of clustering method, the time-space standardization factor, the single linkage termination procedure, thresholds used to inform the SI, the relative weight of the SI components, the minimum cluster flash thresholds and the minimum daily LD storm thresholds. While the SI utilized in this study seems to have provided a satisfactory description of an LD storm, it is very likely that the SI would need to be tailored for use outside of the central Appalachian region of the United States. The index was created by using responses from forecasters who monitor a relatively small region with a somewhat location-specific storm climatology. It is certainly possible that forecasters in different NWSFOs could very well diagnose storm-mode using a different set of weights than those utilized in this study, or that superior results could be obtained using an equal weighting of the index’s inputs. The SI is also limited by the relatively short temporal span used to create the histogram that led to the

delineation of tiers. A longer period of observation would likely provide a smoother, fuller histogram with different tier cut-offs. Further research could focus on expanding both the spatial and temporal areas of consideration.

Chapter 5

Spatial Distributions of Lightning Associated with Low-Shear Thunderstorm Environments in the Central Appalachians Region

by

Paul Miller[1]

Department of Geography
Virginia Tech, Blacksburg, Virginia

[1]Corresponding author address: Department of Geography MC0115, Virginia Tech, 220 Stanger Street, Blacksburg, VA 24061. Email: paulm89@vt.edu

---

Abstract

Differential heating of terrain surfaces has long been observed to play an instrumental role in thunderstorm formation during the summer months. The basic principle behind this phenomenon asserts that a surface's aspect and slope can lead to differential warming by insolation, and consequently, convection is more likely to occur over the warmest terrain that imparts the greatest buoyancy on the air above it. In this study, spatiotemporal cluster analysis was used to group total lightning observations from the ENTLN into likely thunderstorms for the 2012-13 summer seasons over a region of the United States. The storms were then categorized as either a LD single-cell or LD multicell/supercell based on their duration, areal extent, mean velocity and shape. The flashes associated with the 351 LD single-cell storms were then imported into a GIS to compare their frequency against the presence of east- and south-facing surfaces with above average gradients – termed an enhanced diurnal heating surface (EDHS). The influence of EDHSs on total lightning frequency and LD single-cell storm frequency was then examined via a series of pooled *t*-tests at six unique spatial scales. The results indicate that EDHSs possessed a significantly greater frequency of total lightning flashes and LD single-cell storms with the relationship best observed at a 15 km resolution. At this scale, EDHSs possessed 37.6% more single-cell storms than non-EDHSs for the two convective seasons examined.

Keywords: total lightning, differential heating, single-cell thunderstorms, convection

5.1 Introduction

The most unorganized convective mode, a single-cell thunderstorm, is generally defined as a storm forming in an environment characterized by weak vertical wind shear (Markowski and Richardson 2010). In Chapter 4, likely single-cell storms were satisfactorily distinguished from likely multicellular and supercellular storms using total lightning flashes detected by the ENTLN. The study successfully isolated a subset of days possessing a majority of LD single-cell storms which were further characterized by significantly weaker wind shear than LD multicell/supercell days.

The data analyzed in Chapter 4 were collected during the summer of 2012 over an area roughly outlining the Blacksburg NWSFO CWA (Fig. 2a). The domain includes both rugged, mountainous terrain in the west and lower elevation piedmont to the east (Fig. 2b). The highly variable terrain of the study area qualifies the region as an excellent setting in which to observe topographically-induced differential heating patterns within summertime air masses.

The topographic influence on storm initiation and propagation has been well-documented for mountainous terrains dating back several decades (e.g., Hallenbeck 1922; Klitch et al. 1985). Additionally, observations of local Blacksburg NWSFO forecasters cite the heterogeneous topography of their CWA as frequently contributing to preferential storm propagation along differential heating boundaries associated with ridgelines [J. Hudgins, Lead Forecaster, NWSFO Blacksburg, 2013, personal communication]. In the absence of large-scale dynamic forcing mechanisms, diurnal heating is the primary means by which convection is formed (Markowski and

Richardson 2010). Thus, given the previous scientific findings and anecdotal observations, it is thought that the role of the landscape in convective initiation is more apparent on low-shear days, such as those identified in Chapter 4, rather than on days of greater dynamic forcing and more organized convection.

This analysis will utilize the set of single-cell thunderstorms developed through the analysis described in Chapter 4 to examine the relationship between underlying terrain and single-cell thunderstorm formation. Although the previous chapter considered only one summer of lightning activity, it produced the only known data base of single-cell thunderstorms for the central Appalachian Mountains region. To make the results of this particular study more robust, the thunderstorm sample size is expanded to include the 2013 convective season across the central Appalachian Mountains region after applying the analysis methods of Chapter 4. This work focuses on the spatial distribution of the individual LD single-cell thunderstorms relative to the terrain features. Despite the limited record, basic conclusions may be drawn about the preferred spatial distribution of this type of thunderstorm.

5.2 Data

a. Regional Total Lightning and Atmospheric Observations

The same data detailed in Chapter 3 are utilized here with two exceptions. First, ENTLN total lightning observations were expanded to include the 2013 convective season (1 May though 31 August). As referenced in Chapter 3, 2013 flashes were processed under a different version of the detection algorithm than 2012 flashes. However, it was judged that the use of 2012 and 2013 flashes in this analysis, identical

to Chapter 4, would be robust to inconsistencies in detection efficiency and classification efficiency. Since only the X, Y and T coordinates of flashes are utilized in this analysis, any systematic influence exercised by the algorithm upgrade would be minimal. Second, based on the analysis performed in Chapter 4, only 0000 UTC radiosonde observations were obtained for the 2013 season. Since 0000 UTC 0-6 km wind shear was more strongly correlated to median SI score than 1200 UTC 0-6 km wind shear during the 2012 season, only 0000 UTC 0-6 km shear was considered in this expanded analysis.

b. Terrain Data

To represent the topography of the region, a 30 m resolution digital elevation model (DEM) of the study area was obtained from the National Elevation Dataset (NED) through the National Map Viewer download platform (http://viewer.nationalmap.gov/viewer/). The NED is the standard elevation product of the United States Geological Survey (USGS) and is updated bimonthly to incorporate improved source data (Gesch et al. 2009).

5.3 Methods

a. Processing Terrain Data

The DEM was imported into ESRI's ArcMap version 10.1, a GIS platform, for raster processing. While the DEM was originally obtained at a 30 m resolution, it was doubtful that such fine spatial detail would be necessary, or even useful, when considering the spatial tendencies of ordinary thunderstorms. As such, the DEM was re-expressed in seven coarser resolutions: 90 m, ~1 km, ~5 km, ~10 km, ~15 km, ~20 km, and ~25 km. For each of the eight resolutions, the surface slopes (also referred to as

"gradients") and aspects of the DEM rasters were calculated using the standard suite of spatial processing tools available in ArcMap 10.1. For each resulting aspect and slope raster, all cells were reclassified to differentiate between east- and south-facing versus west- and north-facing surfaces as well as below-average slopes versus above-average slopes, respectively.

Aspects between 67.5 and 247.5 degrees clockwise from true north were selected for their prolonged exposure to the summer sun. East-facing slopes are exposed to insolation as soon as it breaks the horizon, and likewise, south-facing slopes are exposed to a component of the sun's rays throughout the day. The study area's latitude north of the Tropic of Cancer places the sun at a southerly angle in the sky, even on the summer solstice. Since small-scale mountain-valley circulations are frequently attributed to the differential heating of slopes beginning in the early morning (Rauber et al. 2008), this 180-degree range of aspects was hypothesized to facilitate diurnal heating due to incoming solar radiation.

High surface gradients have been long observed to associate with enhanced convective activity (e.g., Klitch et al. 1985). For instance, Gambill and Mecikalski (2011) found that steeper gradients are associated with a greater percentage of convective cloud cover than more horizontally-oriented terrains. Thus, the mean slope value of all raster cells at each resolution as generated by the GIS software was designated as the slope threshold. Surfaces with slopes above the threshold would be considered "above-average" and were hypothesized to have a greater influence on ordinary thunderstorm activity than surfaces with slopes below the threshold. For each resolution, cells meeting

both the east- or south-facing aspect and above-average slope qualifications were isolated so their relationship to observed LD single-cell thunderstorm activity could be quantified. From hereon, this class of topography will be referred to as an “enhanced diurnal heating surface” (EDHS).

b. Identifying Single-cell Thunderstorms

The process of identifying single-cell thunderstorms for the 2012-2013 convective seasons (1 May – 31 August) was adopted from Chapter 4. For more details regarding the single-cell thunderstorm classification method, please revisit the previous chapter. It should be recalled that this procedure represents only a preliminary attempt at storm classification via total lightning observations, and the researcher acknowledges that many aspects of the methodology are open to refinement and improvement. This study utilized the exact method outlined in Chapter 4, and consequently, did not attempt to perform any of the improvements suggested by the researcher. Thus, the same potential limitations acknowledged in Chapter 4 should be applied to the results of this analysis as well.

Figure 15 represents the distribution of median SI scores for all 2012 and 2013 storm days, and Table 3 summarizes the results of the LD single-cell and multicell/supercell storm day classification. Of the 246 days during 2012-13 for which data were obtained, lightning was recorded on 178 days (72.4%). As in Chapter 4, a Welch’s analysis of variance procedure (ANOVA) was performed to test the difference in 0000 UTC 0-6 km shear between the two categories for statistical significance. The Welch’s test revealed with 99% confidence that single-cell days possessed significantly

lower wind shear (13.9 knots) than multicell/supercell days (24.4 knots). The result of this procedure suggests that the 25 LD single-cell days identified by the methodology of Chapter 4 represent a statistically significant decrease in 0000 UTC 0-6 km wind shear, consistent with traditional definitions for air mass storms (Markowski and Richardson 2010).

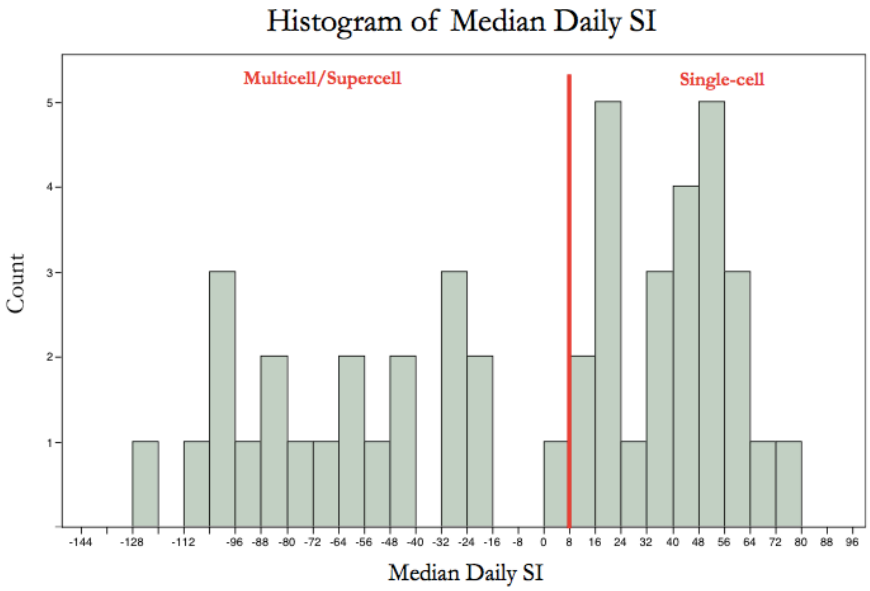

Figure 15. Histogram representing the distribution of median daily SI scores for all 2012 and 2013 days with at least 6 storms of 100 or more lightning flashes.

Category	SI Bounds	Number of Days	Number of LD Storms
Single-cell	> 8	25	351
Multicell/supercell	≤ 8	25	235

Table 3. Divisions of the median daily SI scores that were used to define each category.

It is worth noting that of the 25 LD single-cell storm days, 24 occurred during the 2012 convective season, with the 2013 season contributing only one LD single-cell storm day according to the SI. However, such a result is not unexpected considering the dynamically active atmosphere that characterized the summer of 2013 across the study

area [W. Perry, Lead Forecaster, Blacksburg NWSFO, 2014, personal communication] and the fact that the goal of the methodology is to identify the most clear-cut single-cell storm days.

After isolating LD single-cell thunderstorm days, all flashes associated with LD storms on those days were isolated and imported into ESRI's ArcMap 10.1. The flashes were plotted based on the latitude and longitude recorded by the ENTLN and aggregated into the same eight gridded raster resolutions of the DEM. Additionally, polygons representing the minimum bounding geometry of all 351 storms (i.e., flash clusters) on LD single-cell days were plotted along with their associated flashes.

5.4 Results and Discussion

5.4.1 Convection associated with EDHSs

Pooled *t*-tests were performed on the gridded total lightning flash counts of the reclassified EDHS cells. Table 4 displays the results of the statistical evaluations for each of the eight spatial resolutions. Although the pooled *t*-test suggests a statistically significant difference in flash counts at the 30 m and 90 m resolutions, the statistical significance is likely to be a by-product of the large number of raster cells constituting the sample at these fine resolutions. For these two scales, the relative magnitudes of the mean flash counts disagree with the trends among the six coarser resolutions. For this reason, the statistical significance of the pooled *t*-test conducted using these spatial resolutions is ignored. As the DEM resolution decreases, the mean flash counts match the expectations of the hypothesis although a statistically significant difference in mean flash counts is not observed until the 15 km and ~20 km resolutions. Upon reaching the

coarsest cell size, the difference between ordinary flash counts is no longer statistically significant.

While Table 4 addresses the total flash frequency of LD single-cell thunderstorms across the study domain, this may not necessarily correspond to the actual LD single-cell storm frequency. The results from the previous *t*-tests cannot differentiate between infrequent LD single-cell thunderstorms with a large lighting output and frequent LD single-cell thunderstorms with a moderate lighting output. To make this distinction, the gridded raster maps were reproduced to reflect the frequency of LD single-cell storms over the two-summer study period.

Resolution (m)	EDHS Mean Flash Count	Non-EDHS Mean Flash Count	P-value
30	0.00179	0.00184	<0.0001*
90	0.0157	0.0166	<0.0001*
990	2.02	1.98	0.2749
5,010	54.1	49.1	0.2235
9,990	212.9	182.7	0.2229
15,000	583.2	386.6	0.0016*
19.980	995.2	691.3	0.0432*
24,990	1440.3	1048.9	0.1223

Table 4. Results of the pooled *t*-tests for total lightning flash counts belonging to storms occurring on LD ordinary thunderstorm days. The tests were performed at eight ascending spatial scales between EDHSs and non-EDHSs. * indicates a statistically significant result with 95% confidence.

The same series of pooled *t*-tests performed on the mean total flash counts are applied to the LD single-cell storm counts (Table 5). As with the flash counts, a very low p-value emerges at the finest resolutions. While the mean LD storm count at 30 m is nonetheless significant, the magnitude of the difference is of little practical value. Additionally, the significance promptly disappears as the resolution decreases to 90 m.

Therefore, the conclusion of the *t*-test at 30 m will be ignored for mean LD storm count as it was with regard to mean flash counts. The pooled *t*-tests indicate statistically significant differences in LD single-cell storm frequencies at the ~1 km, ~5 km, ~10 km, and 15 km resolutions with 95% confidence. The statistical significance of the difference in LD storm counts then diminishes below 95% confidence with the ~20 km and ~25 km resolutions.

Resolution (m)	EDHS Mean LD Storm Count	Non-EDHS Mean LD Storm Count	P-value
30	1.379	1.326	<0.0001*
90	1.343	1.335	0.566
990	1.457	1.311	<0.0001*
5,010	1.560	1.298	<0.0001*
9,990	1.583	1.275	0.0096*
15,000	1.727	1.255	0.0105*
19.980	1.519	1.167	0.1272
24,990	1.706	1.297	0.1088

Table 5. Results of the pooled *t*-tests for counts of LD storms occurring on LD single-cell thunderstorm days. The tests were performed at eight ascending spatial scales between EDHSs and non-EDHSs. * indicates a statistically significant result with 95% confidence.

Combining the results of both series of pooled *t*-tests, a 15 km spatial resolution appears to be the ideal level of detail to identify the topographical influences on ordinary convection within this particular study area. Although smaller p-values occur at finer resolutions, the magnitude of the difference between the mean LD single-cell storm count is of little practical meaning at these scales. At 15 km, EDHSs experienced an average of 0.472 more LD storms over the two-summer period, or 37.6% more LD storms than non-EDHSs (i.e., from Table 5, 1.727/1.255 = 1.376). While previous studies have used finer resolutions (~1 km) to derive meaningful relationships, these

studies focused on the frequency of convective clouds, which possess horizontal scales of only several hundred meters (Gambill and Mecikalski 2011). Since thunderstorms capable of producing lightning are considerably wider than these cumuliform clouds, a larger horizontal scale, at least as large as the phenomenon being observed, should be considered (Gibson and Vonder Haar 1990). In their mature stage, robust air mass thunderstorms often grow to diameters in the 10-20 km range (Byers and Braham 1949; Rauber et al. 2008), lending credibility to the statistical significance found at a 15 km resolution. This also serves to further discredit the extremely low p-values observed at very fine scales. Figure 16a depicts an overlay of the EDHS cells identified at the 15 km resolution with the original 30 m DEM, further clarifying the types of surfaces favored for LD single-cell storm development within the study area.

The basic results of this spatial analysis agree well with previous scientific work on this topic. Several studies have focused on the frequency of convective clouds to the terrain beneath them (Gambill and Mecikalski 2011; Gibson and Vonder Haar 1990; Klitch et al. 1985) while others have performed comparable analyses using radar echoes (Kuo and Orville 1973; Outlaw and Murphy 2000). Similar conclusions were reached in these studies – that terrain gradients, rather than absolute elevation, were closely tied to convective initiation. Two explanations are provided within these studies to help elucidate the increased frequency of convective activity along terrain gradients: 1) terrain gradients disrupt surface air flow leading to convergence of air near the surface (Gambill and Mecikalski 2011; Gibson and Vonder Haar 1990; Klitch et al. 1985; Kuo and Orville 1973) and 2) the differential heating of sloped surfaces induces small-

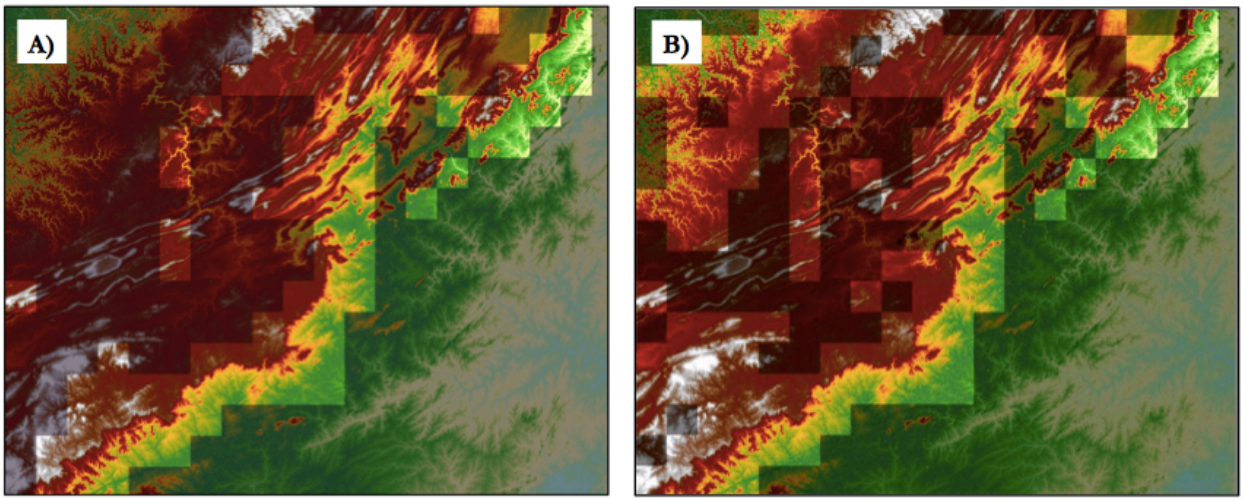

Figure 16. The 30 m DEM of the study area with (a) EDHS cells and (b) "steep" cells identified at a 15 km resolution overlayed as transparent raster cells.

scale mountain-valley circulations that can enhance updraft development (Gambill and Mecikalski 2011; Outlaw and Murphy 2000).

While a greater frequency of ordinary convection was observed within EDHS cells, it is possible that the formation of thunderstorms over these terrains was aided by low-level wind fields as suggested by previous research (e.g., Kuo and Orville 1973). In cases of easterly or southerly low-level flow (surface to 850 hPa), storm initiation due to orographic lift could cause a similar distribution of ordinary thunderstorms as those induced by differential heating. However, 0000 UTC RNK radiosonde observations indicate that surface and 850 hPa wind directions on the 25 LD ordinary thunderstorm days do not demonstrate an easterly or southerly bias (Fig. 17). Thus, the differences in mean total flash counts and mean LD single-cell thunderstorm counts between EDHS and non-EDHS cells can be attributed to topographically-induced differential heating processes with increased confidence.

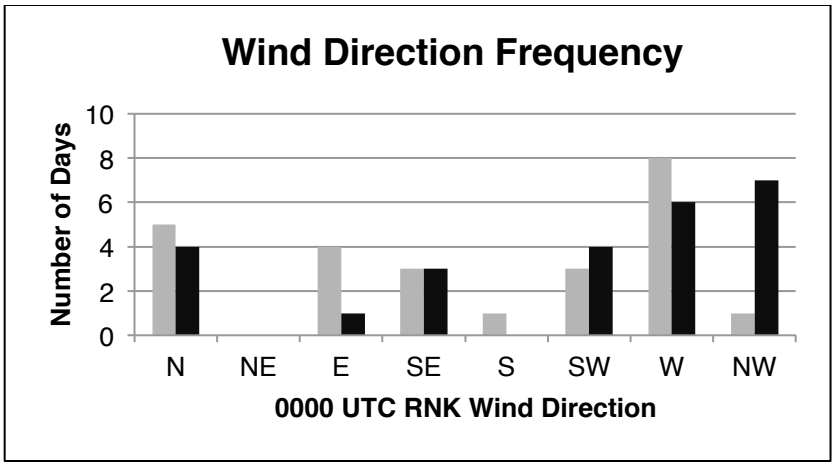

Figure 17. Counts of surface (gray) and 850 hPa (black) wind directions on LD single-cell thunderstorm days. Wind directions were determined from 0000 UTC KRNK radiosonde observations.

5.4.2 The Role of Surface Aspect in Convective Frequency

Many of the previously cited studies clearly acknowledge the role of terrain gradient in thunderstorm initiation (e.g., Outlaw and Murphy 2000; Gibson and Vonder Haar 1990; Gambill and Mecikalski 2011), and all agree that steep terrain gradients contribute to the differential heating processes that increase instability and parcel buoyancy. However, none actively investigate the influence of terrain aspect on subsequent thunderstorm activity. While it might be implied that in order for differential heating to occur the orientation of the surface is relevant, there is no explicit consideration of the aspects of terrains that support the greatest convective frequency.

It is likely that the implicit discussion of aspect, but the explicit analysis of only gradient, is related to the location of the topographically-induced convergence zone. Though surface aspects contribute to the formation of small-scale circulations, the convergence cause by these circulations will be maximized along the ridgetop rather than a particular aspect. Any thunderstorm forming over a sufficiently sloped terrain, will likely appear as if it formed directly above the ridge rather than a particular slope. To

investigate the analytical benefit (if any) of including aspect as an EDHS criteria, the previous analysis was re-conducted solely for above-average ("steep") versus below-average ("non-steep") slopes. Tables 4 and 5 were reproduced to express the results of the "slope only" analysis for both total lightning flash counts (Table 6) and LD single-cell storm counts (Table 7).

Resolution (m)	Steep Mean Flash Count	Non-steep Mean Flash Count	P-value
30	0.001804	0.001846	<0.0001*
90	0.1575	0.01688	<0.0001*
990	2.026	1.962	0.0477*
5,010	51.72	49.18	0.4642
9,990	195.32	186.98	0.7036
15,000	487.5	406.5	0.2136
19.980	838.87	743.09	0.4963
24,990	1208.33	1151.41	0.8131

Table 6. Results of the pooled *t*-tests for total lightning flash counts belonging to storms occurring on LD single-cell thunderstorm days. The tests were performed at eight ascending spatial scales between steep and non-steep surfaces. * indicates a statistically significant result with 95% confidence.

Resolution (m)	Steep LD Storm Count	Non-steep Mean LD Storm Count	P-value
30	1.384	1.305	<0.0001*
90	1.346	1.331	0.1721
990	1.438	1.285	<0.0001*
5,010	1.464	1.290	0.0014*
9,990	1.409	1.317	0.3857
15,000	1.533	1.278	0.1314
19.980	1.338	1.226	0.6052
24,990	1.375	1.500	0.6057

Table 7. Results of the pooled *t*-tests for counts of LD storms occurring on LD single-cell thunderstorm days. The tests were performed at eight ascending spatial scales between steep and non-steep surfaces. * indicates a statistically significant result with 95% confidence.

The same low total flash count p-values that were found at very fine resolutions in Table 4 are evident in Table 6 as well. Likewise, a very similar pattern of LD single-cell storm count p-values for the 30 – 5010 m resolutions can be found in Tables 5 and 7. However, as mentioned during the EDHS analysis, it is hypothesized that the high statistical significances identified at these fine resolutions is a result of the extremely large sample size (number of cells) involved with the calculations at these resolutions. The similarities between the two evaluations can be understood more clearly by comparing the cells involved in each set of calculations. Figure 16b illustrates that many of the "steep" raster cells at the 15 km coarseness were also EDHS cells (Fig. 16a).

While the overall results of the two analyses were comparable, the most obvious difference lies in the lack of statistical significances in the coarser resolutions of Tables 6 and 7. Though Tables 4 and 5 suggest that a 15 km resolution was the most appropriate scale at which to compare the storm-terrain relationship, neither Table 6 nor 7 indicate a statistically significant relationship between terrain slope and convective frequency at this resolution. While it would thus appear there is some value to explicitly considering the aspect of the terrain when identifying convection-enhancing surfaces, it should be noted that these results somewhat disagree with observations from glider pilots and other modeling studies (Federal Aviation Administration 2013).

5.5 Conclusions

Single-cell air mass thunderstorms represent the most disorganized, yet most frequent, summertime convective mode in the central Appalachian Mountains region. Despite the seasonal decline of upper level dynamical support across the southeastern

United States during summer months, little research has focused specifically on the thunderstorms that form in a weakly-sheared environment. This analysis utilized a recently developed methodology for identifying low-shear environments based on the spatiotemporal distribution of total lightning flashes (Ch. 4) to examine the spatial distribution of storms occurring on LD single-cell thunderstorm days. The results, though basic and stemming from a limited thunderstorm sample, confirm many previous findings as well as anecdotal forecaster observations.

LD storms occurring on the 25 LD single-cell thunderstorm days during the 2012-2013 convective seasons showed a clear tendency to occur over east- and south-facing terrain with above average surface slopes. This result has been well established by previous studies examining terrain influences on the formation of convective clouds. Identifying key areas of preferred convective activity in low-shear summer environments could be of great operational value to local forecasters, especially in the heterogeneous terrain of the Blacksburg NWSFO CWA.

It is important to note that the results of the analysis were based on only two years of total lightning data. While apparently meaningful patterns did emerge during the study, a longer period of consideration could possibly yield different or, at a minimum, more reliable results. Further research could benefit from examining the spatial distribution of single-cell thunderstorms under varying surface conditions similar to Kuo and Orville (1973) whom examined the frequency of radar echoes over heterogeneous terrain in for various cases of wind flow direction.

Chapter 6

The Utility of Total Lightning Trends in Diagnosing Single-cell Thunderstorm Severity in the Central Appalachians Region

by

Paul Miller[1]

Department of Geography
Virginia Tech, Blacksburg, Virginia

[1]Corresponding author address: Department of Geography MC0115, Virginia Tech, 220 Stanger Street, Blacksburg, VA 24061. Email: paulm89@vt.edu

---

Abstract

This chapter evaluates the performance of total lightning jump-based storm warnings within a weakly sheared environment. Total lightning observations from the ENTLN during the summer of 2012-13 (1 May – 31 August) for a study domain within the central Appalachians region were clustered into likely thunderstorms using single linkage clustering. The spatial and temporal characteristics of each flash cluster were then evaluated, and all clusters were assigned an SI score along a linear scale beginning at 100 and decaying past zero. Small, short-lived, slow-moving, circular clusters – consistent with single-cell thunderstorms – were given high scores while large, long-lived, fast-moving, linear clusters – inconsistent with the single-cell mode – received low scores. Days with a simple majority of LD single-cell storms possessed statistically significant weaker 0000 UTC 0-6 km wind shear than days with a majority of non-single-cell storms. After classifying 470 clusters as either LD single-cell or LD multicell/supercell the 2σ lightning jump algorithm (Schultz et al. 2011) was applied to all flashes associated with each cluster. Total lightning jumps identified by the algorithm were compared against severe weather reports from *Storm Data* to evaluate the accuracy of the algorithm. While PODs for both categories compared well to previous studies, FARs were significantly higher than previously documented. Though the algorithm did not perform satisfactorily among LD single-cell or LD multicell/supercell storms, its performance deteriorated even further when applied to a subset of LD storms with SI scores very near 100.

Keywords: total lightning, lightning jump, thunderstorm mode, weak shear

6.1 Introduction

As discussed in Chapter 1, recent total lightning severe weather research has focused around the "total lightning jump" – referencing a sharp increase in the total flash rate of a thunderstorm prior to the manifestation of severe weather[1]. Once the reliability of the "jumps" identified in early total lightning studies (e.g., Goodman et al. 1988; Goodman et al. 2005; MacGorman et al. 1989; Williams et al. 1999) was asserted by later research, efforts shifted to begin quantifying the increase in total flash rate that constitutes a jump (Gatlin and Goodman 2010; Schultz et al 2009). With the first formulation of an LJA by Gatlin and Goodman (2010) and refined by Schultz et al. (2009, 2011), there exist several definitions for the increase in total flash rate that forms a jump. The "2σ" version of the algorithm (Schultz et al. 2009, 2011), so named for its requirement that the current flash rate exceed two standard deviations of the running mean flash rates, has proven to be the most reliable among all the tested versions of an LJA. However, recently attention has shifted from establishing the consistency of LJAs to testing their transferability to other geographic regions (Rudlosky and Fuelberg 2013), assessing the operational value to forecasters (Darden et al. 2010), and applying the algorithm in conjunction with non-lightning derived measurements (Rudlosky and Fuelberg 2013).

While the development and verification of LJAs is still in its infancy, there are nonetheless many questions that need to be answered before an LJA can be formally utilized by operational forecasters. One such concern voiced by previous studies is the

[1] The National Weather Service defines a severe thunderstorm as one producing at least one of the following: a tornado, hail greater than or equal to 1 in (2.54 cm) in diameter, or winds greater than or equal to 58 mi hr^{-1} (93.3 km hr^{-1}).

transferability of the algorithm to a broader range of meteorological regimes than those considered to-date. However, no LJA study has sincerely heeded the advice of previous authors, and there has been little focused attention to the convective regimes in which the storms form. While two studies have included brief discussions of the algorithm's performance among different storm modes (Goodman et al. 2005; Schultz et al. 2011), no research yet has provided detailed documentation of an LJA's performance as a function of convective environment. Consequently, the purpose of this study is to assess the transferability of the 2σ algorithm to weakly-sheared atmospheres that support disorganized single-cell thunderstorms during the summer months.

Many of the previous lightning jump studies were conducted using regional LMAs, and consequently, the results represent a narrow range of spatial domains and severe weather climatologies (Fig. 18). In contrast, this study considers the mountainous terrain of the Central Appalachians and its neighboring piedmont (Fig. 2) and offers explicit focus on single-cell thunderstorms forming in low-shear environments. To accomplish this, the 2σ jump detection algorithm is applied to storms that occurred within summertime regimes characterized by statistically significant lower shear (Ch. 4, 5). In the method outlined in Chapter 4 and utilized in Chapter 5, the identification of LD single-cell and multicell/supercell thunderstorm days during a summer season for a region of the eastern United States was predicated on the spatiotemporal distribution of total lightning.

The data analyzed in this study were collected during the summers of 2012-2013 over an area roughly outlining the Blacksburg NWSFO CWA (Fig. 2a). Chapter 5 utilized

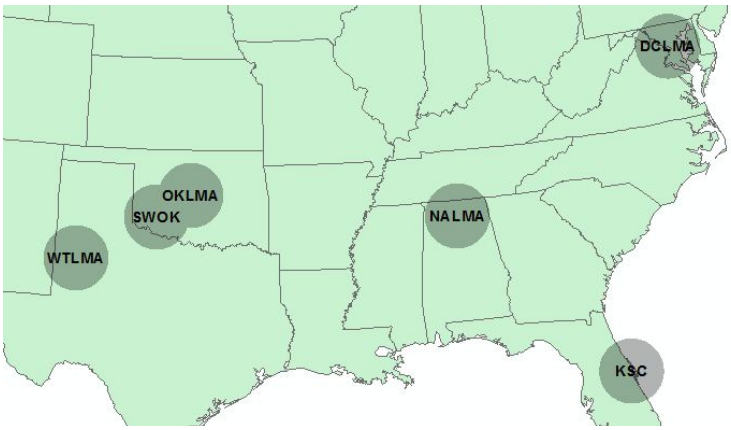

Figure 18. The geographical distribution of current LMA operational domains (adapted from Filiaggi 2012). An additional eastern Colorado-western Kansas study area included in Schultz et al. (2011) is not shown.

this same set of observations, but considered only the spatial distribution of LD single-cell storms and their associated flashes. This chapter will study the temporal trends of flashes within both LD single-cell and LD multicell/supercell storms with a clear focus on the ability of the 2σ algorithm to precede severe weather events produced by LD single-cell storms. The results of this study will allow forecasters to better understand the transferability of the 2σ jump detection to low-shear convective regimes.

6.2 Data

a. Total Lightning Data

ENTLN observations for both the 2012 and 2013 convective seasons were utilized for the analysis described in this chapter. However, as discussed in Chapter 3, the ENTLN detection algorithm was upgraded during the winter of the 2012-13. Consequently, the two-year study period selected by the researchers (prior to any ENTLN algorithm upgrade plans) represents data of inconsistent integrity. Since the upgrade to the ENTLN algorithm increased detection efficiency and classification efficiency (Mallick et al. 2013), it was decided that combining both 2012 and 2013

lightning flashes into a single sample could potentially adversely influence the robustness of the results of this portion of the thesis research. Even though the storm mode classification technique outlined in Chapter 4 was conducted in its entirety on both years of total lightning data in Chapter 5, only data from the 2012 season is included in the results section of this chapter. The argument for excluding 2013 ENTLN observations will be discussed in the methods section.

b. Severe Weather Reports

Severe weather reports were obtained through the National Climatic Data Center's (NCDC) *Storm Data* publication. While an effort is made to quality-control the reports published within *Storm Data*, the NWS does not guarantee the accuracy of the reports (National Climatic Data Center 2013). While several studies have documented temporal inconsistencies and spatial errors in the reporting of severe weather (e.g., Williams et al. 1999; Witt et al. 1998a, b), it must also be acknowledged that some severe weather events may not be documented at all. Despite these issues, *Storm Data* is generally regarded as the most accessible and respected severe weather dataset available for analysis.

6.3 Methods

6.3.1 Identifying Single-cell Thunderstorm Days

The process of identifying single-cell thunderstorms for the 2012-2013 convective seasons (1 May – 31 August) was adopted from Chapter 4 and applied in the analysis described in Chapter 5. Though Chapter 5 was only concerned with the LD single-cell elements of the sample, this chapter will consider storms of both modes – LD single-cell

and LD multicell/supercell. For more details on the storm mode identification process, see Chapter 4.

Once again, it is necessary to state the limitations of the lightning-based storm mode identification efforts. Chapter 4 represents only a preliminary attempt at storm classification via total lightning observations, and the researcher acknowledges that many aspects of the methodology are open to refinement and improvement. This study utilized the exact method outlined in Chapter 4, and consequently, did not attempt to perform any of the improvements suggested by the researchers. Thus, the same limitations stated within Chapter 4 should be applied to the results of this analysis as well.

Figure 19a duplicates Figure 15 from Chapter 5, and Table 3 summarizes the results of the LD single-cell and multicell/supercell storm day classification for 2012-2013. It was mentioned in Chapter 5 that a Welch's test revealed with 99% confidence that LD single-cell days possessed significantly lower wind shear (13.9 knots) than multicell/supercell days (24.4 knots). As described in Chapter 4, to be classified as an "LD single-cell thunderstorm day", the median SI for a day with at least six, 100-flash clusters must have fallen within the top tier of median SI scores according to the SI histogram. While it is possible (and, indeed, it is so) that LD storms with very low SI scores occurred on LD single-cell thunderstorm days, the "average" LD storm on these days was nonetheless satisfactorily short-lived, small, slow-moving and circular.

As mentioned in Chapter 3 and the data section of this chapter, the above methodology, performed on two full convective seasons, was conducted on ENTLN data

of inconsistent integrity. Though it is expected that the spatial (areal extent, shape) and temporal attributes (duration, mean velocity) of total lightning clusters may be relatively

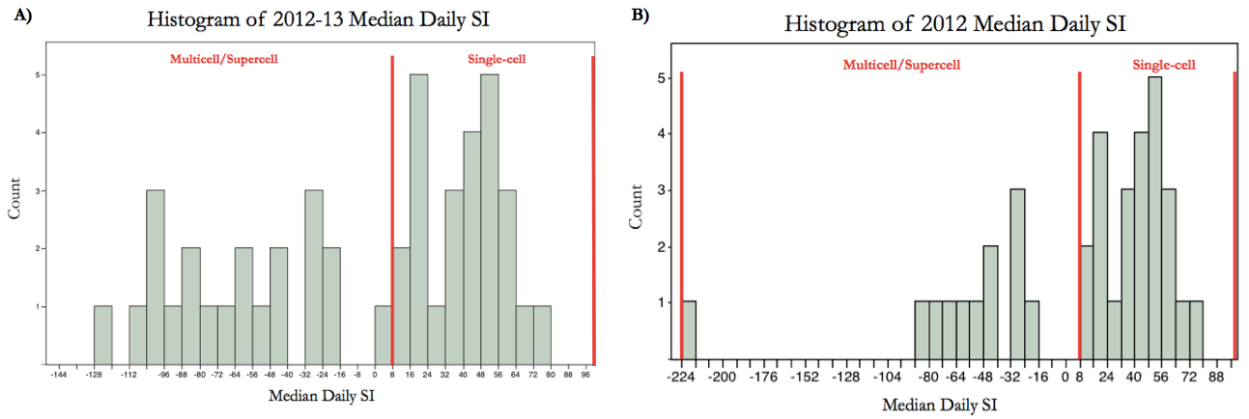

Figure 19. Histogram of median daily SI scores for the a) 50 storm days during the summer of 2012-2013 and b) 36 storm days during the summer of 2012. A median SI score of 8 served as the division between LD single-cell and LD multicell/supercell thunderstorm days.

robust to changes in ENTLN detection efficiency and classification efficiency, the time series of total lightning activity (including the presence/absence of total lightning jumps) may be much more sensitive to these changes. Since the above analysis identified a much greater number of LD single-cell days from 2012 than 2013, it was decided that removing 2013 clusters from any further analysis would greatly increase the consistency of the ENTLN data used while minimally reducing the sample size of LD single-cell storms. Figure 19b and Table 8 re-express the results of the clustering method for the 2012 season alone.

Category	SI Bounds	Number of days	Number of LD Storms
LD Single-cell	> 8	24	334
LD Multi/Super	≤ 8	12	136

Table 8. Same as Table 3, but only represents results for 2012.

6.3.2 The Lightning Jump Algorithm

The first generation of LJAs were developed by Gatlin and Goodman (2010) whom evaluated 10 000 unique combinations of possible LJA configurations. The work of Schultz et al. (2009, 2011) built upon the results of Gatlin and Goodman (2010) by evaluating the performance of six LJAs. After rigorous testing, it was determined the "2σ algorithm" possessed the best combination of FAR and POD (Schultz et al. 2009).

As explained in great detail by Schultz et al. (2011), under this configuration of the algorithm, the two most recent 1-min lightning periods are averaged together forming a 2-min flash rate average expressed in flashes min^{-1} (fpm). If this average exceeds 10 fpm the algorithm executes. Upon activation of the algorithm, six 2-min averages are calculated from the 12 min of total lightning activity prior to the most current 2 min. Consecutive 2-min averages are then subtracted yielding five values representing the time rate of change of the total flash rate, DFRDT ($\Delta FR/\Delta t$; flashes min^{-2}). A standard deviation (σ) is computed from these five values, and the jump threshold is set equal to twice this value (2σ). The 2-min average immediately prior to the most current 2-min average flash rate is subtracted from the most current 2-min average itself, resulting in the current DFRDT value. If this new value exceeds the jump threshold, then a lightning jump is deemed to have occurred. Figure 20 depicts an example of a typical flash rate time series.

6.3.3 Assessing Storm Severity and LJA Performance

To establish a binary classification of storm severity, the locations of severe weather reports were compared to the spatial footprint of every LD storm's total lightning

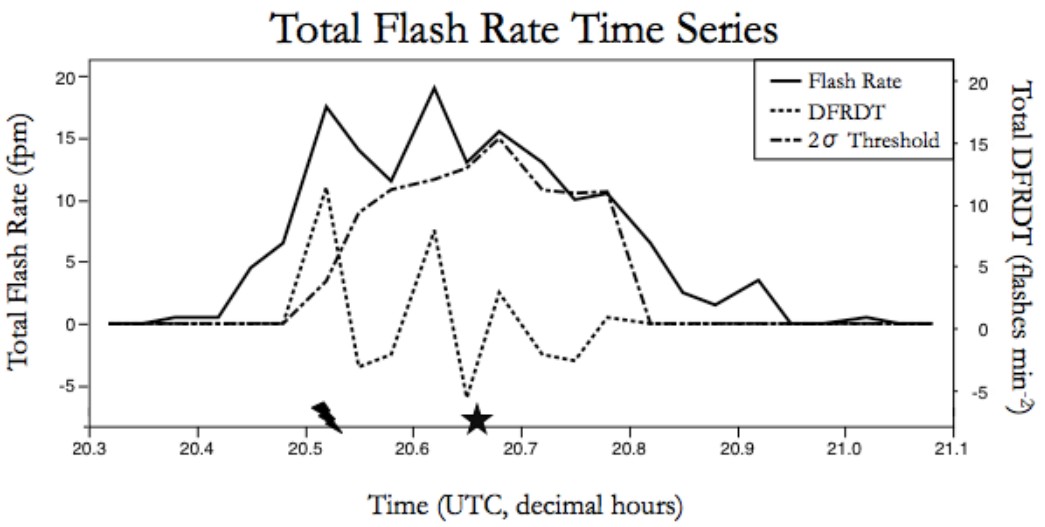

Figure 20. Flash rate time series of a thunderstorm occurring on 8 July 2012. The total lightning jump is marked by a lightning bolt, and the corresponding severe weather event is marked by a star on the horizontal axis. The vertical axes represent values for two different units. When interpreting flash rate, the vertical axes represent fpm, but when interpreting DFRDT and 2σ thresholds, the axes represent flashes min^{-2}.

activity within a GIS interface. ESRI's ArcMap 10.1 served as the GIS platform for the spatial components of this study's analysis. Successful spatial joins were then isolated to only include those joins whose severe weather report occurred after the first lightning flash but before the last lightning flash in a cluster. A storm was then deemed severe if a severe weather report fell within an LD storm's spatiotemporal bounds. If no severe weather report occurred within these bounds then the LD storm was deemed nonsevere.

It should be noted that there were several possible sources of error introduced in the spatiotemporal joining stage. For instance, many widespread severe weather-producing storms were excluded from the 470- LD storm pool since they occurred partially outside of the study domain, and thus, only partial total lightning data existed for these storms. Additionally, it is possible that a severe weather event either fell outside of

its storm's spatiotemporal lightning footprint, or it was produced by a cluster of less than 100 flashes. Finally, reporting errors (both spatial and temporal) within the *Storm Data* publication could prevent the joining of severe weather event to its parent storm. While there is great confidence that the 53 storms joined to severe weather events produced severe weather, it is possible that at least some of the remaining 417 storms not connected to a severe weather report did indeed produce severe weather. For this reason, it is with great caution that the terms "severe" and "nonsevere" will be used throughout the rest of the analysis.

The assignment of severe weather reports to their parent storms allows for an evaluation of the performance of the 2σ total lightning jump algorithm. Following the methodology outlined by Schultz et al. (2011) once a lightning jump was identified, a "warning" was placed on the storm for the next 45 minutes. If the storm produced a documented severe weather event within the warning window then the severe event was "detected" and the responsible jump was "verified." If a severe weather event occurred without a preceding jump, it was considered "undetected," and if a jump occurred without a subsequent severe weather event within the warning window, it was deemed "unverified." In order to avoid over-estimating the LJA's detection capability, severe weather reports joined to the same storm and occurring within six minutes of each other were combined into a single severe weather event (Schultz et al. 2011). If more than one warning had been issued on a storm upon the observation of a severe weather event, then the verification was applied to the earliest issued warning (Schultz

et al. 2011). Severe weather reports could not be used to validate any overlapping warnings until the earliest issued warning had expired.

To summarize the performance of the algorithm, the following four quantities were computed: POD, FAR, critical success index (CSI), and lead time. The POD, FAR, and CSI were calculated independently for the two storm categories via the following formulas:

$$POD = DETECTED / (DETECTED + UNDETECTED)$$

$$FAR = UNVERIFIED / (VERIFIED + UNVERIFIED)$$

$$CSI = VERIFIED / (VERIFIED + UNVERIFIED + UNDETECTED)$$

Lead time was computed by subtracting the time at which a lightning jump began from the timestamp of the subsequent severe weather event as recorded within *Storm Data*.

6.4 Results and Discussion

The 2σ algorithm was applied to all flashes associated with each of the 470 LD storms as determined according to the methodology from Chapter 5. The results will be presented and discussed as they relate to three areas: SI category, storm severity, and exclusively LD single-cell thunderstorms.

6.4.1 Lightning Patterns by SI Category

Table 9 depicts the total lightning temporal characteristics of both LD storm modes. A cursory glance reveals that while subtle fluctuations exist between values for LD single-cell and LD multicell/supercell storms, there are no obvious differences between the lightning behaviors of the two groups. This qualitative observation is confirmed via a series of pooled *t*-tests for equal variances which identified no

statistically significant differences between the two storm modes for their maximum total flash rates (FRs), mean DFRDT values, or mean jumps per LD storm. The distributions of these max FRs and mean DFRDTs are depicted in Figures 21a and 21b, respectively. Also calculated for each category are the proportions of storms exceeding the minimum FR threshold required to activate the 2σ algorithm (Schultz et al. 2011), the proportion of storms producing at least one jump, and the mean number of jumps per storm; however, there are no distinct differences between LD single-cell and LD multicell/supercell storms.

Category	Mean Max FR	Fraction with Max FR ≥ 10 fpm	Mean Jumps Per LD Storm	Fraction Producing Jumps	Mean DFRDT
LD Single-cell	28.9	83.5	1.00	67.6	9.42
LD Multi/Super	32.6	84.6	1.18	72.1	8.71

Table 9. Mean maximum total lightning FRs of all storms in each category, expressed in fpm. The fractions of storms with maximum FRs meeting the FR thresholds established by Schultz et al. (2011) to activate the LJA are shown as a percentage. Fractions of storms producing total lightning jumps are expressed as percentages, and the mean DFRDT values (flashes min^{-2}) represent the mean value of DFRDT recorded during the entire extent of all a storm's active lightning jumps (i.e, mean jump magnitude).

With all metrics relating to the occurrence of total lightning jumps consistent across the two LD storm modes, attention shifted to evaluating the accuracy of the 2σ algorithm in each group. As explained previously, severe weather reports from *Storm Data* were intersected with the time and space extents of all 470 LD storms as determined through the SI identification method (Chapter 4) using a GIS platform. *Storm Data* yielded 293 severe weather reports within the study domain on LD single-cell or multicell/supercell days that occurred between 1805 UTC and 0100 UTC (Table 10). Of these, 102 occurred within the spatiotemporal total lightning extent of a thunderstorm.

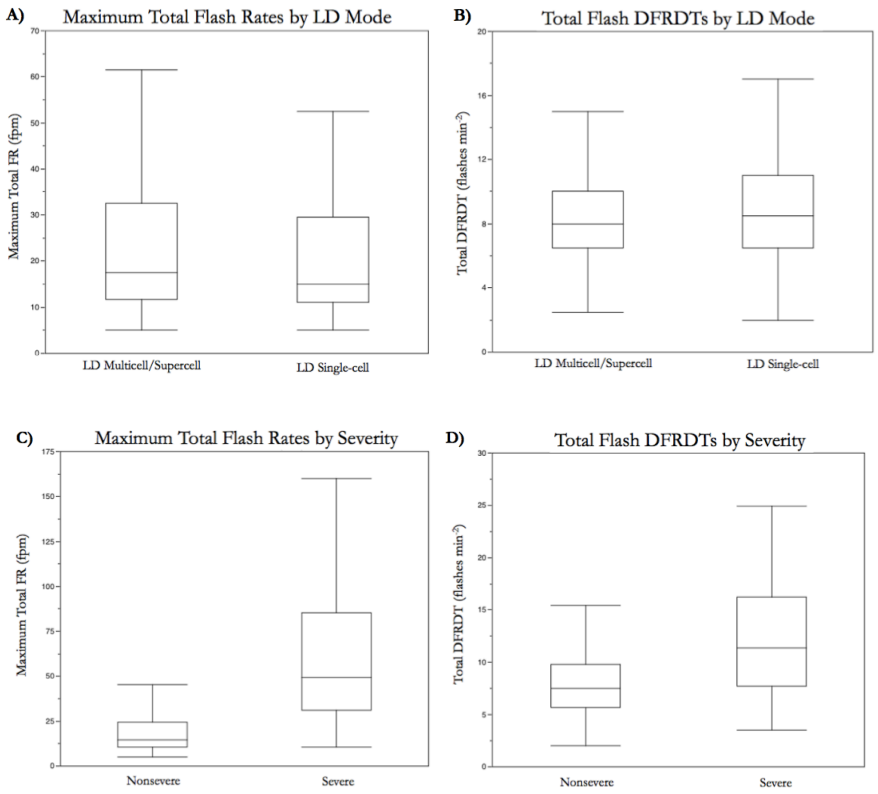

Figure 21. Box plots of (a) maximum total flash rates by LD storm mode, (b) total DFRDTs by LD storm mode, (c) maximum total flash rates by severity and (d) total DFRDTs by severity. Outliers are not shown.

Following the methodology of Schultz et al. (2011), reports occurring within six minutes of each other were combined into a single severe weather event. This consolidation yielded 85 unique severe events produced by 53 different LD storms. By category, 10.5% (35 / 334 = 0.105) of storms on LD single-cell days and 13.2% (18 / 136 = 0.132) of storms on LD multicell/supercell days were linked to severe weather events. Overall, 34.8% of all severe reports were successfully paired with a storm. Possible causes for unmatched *Storm Data* reports were discussed in the Methods section.

Following the incorporation of *Storm Data*, it was possible to quantify the performance of the algorithm in detecting subsequent severe weather events. Table 11

Category	Severe Hail Report	Severe Wind Reports	Total Severe Reports	Mean Reports Per LD Storm	LD Storms with Severe Event
LD Single-cell	48	109	157	0.47	35
LD Multi/Super	62	74	136	1.00	18
Total	*110*	*183*	*293*	-------	*53*

Table 10. Raw severe hail, severe wind, and the sums of both recorded per each SI category. The mean reports per LD storm were calculated by divided the total number of raw reports occurring on all respective SI categorical days by the total number of LD storms in each category.

summarizes the POD, FAR, and CSI for each of the convective categories. While portions of these results compare very well to previous LJA studies, the FAR and CSI values determined by this analysis are in gross disagreement with the 36% FAR and 55% CSI found by Schultz et al. (2011). It is difficult to identify a single likely cause of this discrepancy. Though the methodology utilized to define storm cells and the total lightning observation systems both differ from Schultz et al. (2011), one would hope that for the sake of operational utility, any form of an LJA would be robust to such changes.

Category	Severe Events	Tot. POD	Tot. FAR	Tot. CSI	Mean Tot. Lead Time ± Std. Dev.
LD Single-cell	59	88.1	86.7	12.9	22.15 ± 12.15
LD Multi/Super	26	80.8	90.0	9.7	23.42 ± 14.69

Table 11. Severe weather events for each SI category reflecting the number of severe instances after combining reports occurring within six minutes of each other. POD, FAR, CSI (percentages) and lead time (minutes) were calculated according to the procedures described in the methods section.

Even though the PODs found with this analysis (88.1% for LD single-cell and 80.8% for LD multicell/supercell) resemble those calculated by Schultz et al. (2011) (78.1% for all storm types), the much larger FARs acted to decrease CSIs to near 10%. Additionally, while lead times for severe weather events detected by total lightning

jumps were very comparable to Schultz et al. (2011), their large standard deviations remove most practical meaning from the mean lead times. It should be noted, however, that lead time is very sensitive the timestamp of the severe weather given within Storm Data. Frequently, severe weather will be reported more promptly when storms occur near populated areas whereas reports are less frequent from rural locations. Although performance statistics were somewhat expected to fluctuate across the LD categories, the excessive FARs within both convective environments are certainly disconcerting.

6.4.2 Severe versus Nonsevere Thunderstorm Lightning Trends

After pairing severe weather events to responsible thunderstorms, it is also possible to compare the lightning behaviors of severe thunderstorms against their nonsevere counterparts. The separation of storms into severe and nonsevere categories can provide further insight toward the potentially unique lightning behavior of dangerous thunderstorms. While severe thunderstorms were successfully paired with a severe weather event, it is possible that some “nonsevere” thunderstorms did, in reality, produce severe weather. However, based on the trends expressed in Table 12, the inclusion of severe storms in the nonsevere category would likely only inflate the nonsevere thunderstorm metrics closer to the severe values. Thus, the trend itself would likely remain unaffected by any misclassifications; only the magnitude of the difference would be influenced.

Pooled *t*-tests for unequal variances confirm statistically significant differences in mean maximum total FR and mean total DFRDT between severe and nonsevere storms

Category	LD Storm Count	Fraction Producing Jump	Mean Max FR	Tot. Jumps Per LD Storm	Tot. Jumps Per Hour	Mean DFRDT
Nonsevere	417	65.5	22.10	0.90	1.13	8.35
Severe	53	96.2	78.93	2.25	1.47	13.80

Table 12. Values in this table were produced in identical fashion to their corresponding quantities in Table 9 and are displayed in the same units.

with 95% confidence. The distributions of these two quantities are depicted in Figures 21c and 21d. The max FR measures confirm the results of many previous studies in which severe thunderstorms were characterized by greater FRs than nonsevere storms (e.g., Williams et al 1999; Schultz et al. 2011; Rudlosky and Fuelberg 2013).

The recent work of Rudlosky and Fuelberg (2013) focuses on lightning and radar-derived measurements of a large sample of both severe and nonsevere storms within a nearby geographic region, and thus, the results of their work will provide a useful standard of comparison. Table 13 replicates Table 12 except that all values reflect the work of Rudlosky and Fuelberg (2013). Comparing these two tables, the results are reasonably consistent. While Rudlosky and Fuelberg (2013) did not calculate POD, FAR, CSI or lead time, the study did determine somewhat similar values for the fraction of nonsevere storms recording a total lightning jump. This fraction, 65.5% from this current analysis and 53.7% from Rodlosky and Fuelberg (2013), is a key statistic contributing to the aforementioned high 2σ algorithm's FAR. Ideally, 0% of nonsevere storms would produce total lightning jumps while 100% of severe storms would produce total lightning jumps in a 1:1 ratio with severe weather events. In order for the FAR of an LJA to be reduced toward operationally acceptable levels, this fraction will need to be reduced.

Category	Fraction Producing Jump	Tot. Jumps Per Hour	Mean Tot. DFRDT
Nonsevere	53.7	0.92	9.9
Severe	83.9	1.44	15.9

Table 13. Same as Table 12, but with values taken from Rudlosky and Fuelberg (2013)

Figure 22 displays the distributions of SI scores for severe thunderstorms in each of the LD storm mode categories. Most noteworthy is the distribution of SI scores for severe LD single-cell storms. These storms were broadly defined as thunderstorms occurring on days in which the median cluster fell within the spatial and temporal limits of a plausibly single-cell storm. However, Figure 22a is compared to Figure 22b it is evident that the majority of severe LD single-cell storms (also known as pulse thunderstorms) were unlike most LD single-cell storms. In fact, only 31.4% of LD pulse storms possessed SIs greater than zero, the lower cut-off for a plausibly single-cell thunderstorm. Practically, this means that most LD pulse storms were larger, longer-lasting, more linear, and faster-moving than typical single-cell thunderstorms. Figure 22c displays the distribution of SI scores by storm severity, and confirms expectations that severe storms are much more organized according to the SI than nonsevere storms. While in this study LD single-cell storms were broadly defined as LD storms occurring on LD single-cell days, the trends in Figure 22 suggest that future research could compare severe LD single-cell storms to radar imagery to determine whether they would also be classified as single-cells under radar-based classification criteria.

6.4.3 Lightning Trends in Single-cell Thunderstorms

Up to this point, statistics have been provided for both LD storm modes to provide additional context for the LD single-cell values. However, the purpose of this

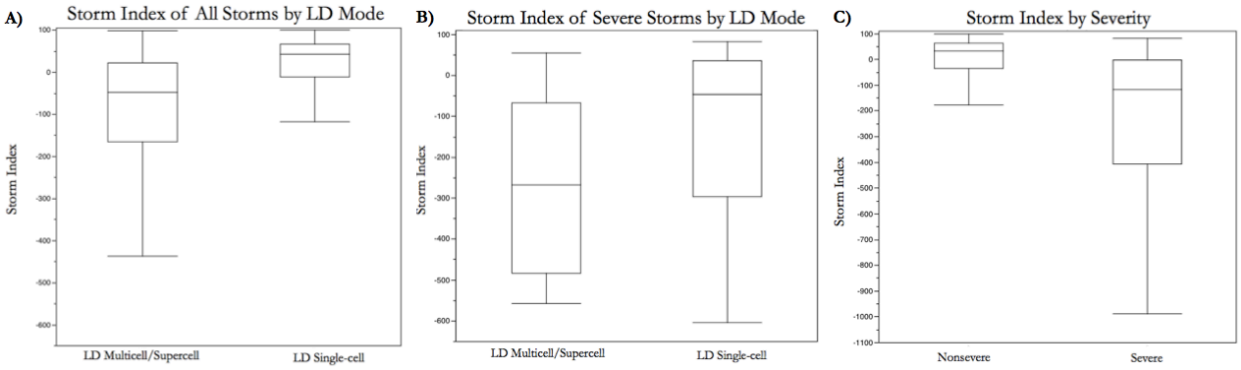

Figure 22. Box plots of SI scores for (a) all LD storms by mode, (b) severe LD storms by storm category and (c) all LD storms by severity. Outliers are not shown.

chapter is ultimately to assess the utility of the algorithm in a low-shear environment. Thus, summary statistics were generated for the 140 storms occurring on LD single-cell storm days whose SI scores were greater than or equal to 50 (Table 14). This sample represents storms that adhered very closely to the expected spatiotemporal characteristics of a single-cell thunderstorm that also occurred on days in which the majority of observed storms also adhered very closely to the spatiotemporal characteristics of a single-cell. Since some storms within the LD single-cell category might actually represent multiple updrafts that developed into a multi-cell cluster, the SI threshold was applied to help ensure that these 140 storms did not possess additional organization that is uncharacteristic of a pure single-cell thunderstorm.

Mean Max FR	Fraction with Max FR ≥ 10 fpm	Mean DFRDT	Fraction Producing Jump	Jumps Per LD Storm	FAR	POD
15.6	80.0	8.45	58.6	0.69	94.8	75.0

Table 14. Summary statistics for the 140 LD single-cell storms with SI scores greater than or equal to 50. All quantities were calculated in an identical fashion and expressed in the same units as those in previous tables.

The results in Table 14 indicate that the subset of purest LD single-cell storms are less electrically active compared to the broader group of storms occurring on weakly-sheared environments. Six of the seven values displayed in Table 14 are less than their corresponding values for the larger LD single-cell category while the only greater quantity, FAR, reflects a poorer performance of the algorithm. The visual trends are confirmed with pooled *t*-tests for unequal variances which identified statistically significant decreases in max FR as well as the number of total lightning jumps per LD thunderstorm with 95% confidence. When compared to the LD multicell/supercell category, max FRs and the number of total lightning jumps per LD storm for the 140-storm subset also possessed a statistically significant decrease.

It should be noted that the inferior performance of the algorithm within this subset of the clearest LD single-cell storms is closely related to the number of severe storms within the sample. Whereas 10.5% (35 / 334 = 0.105) of storms in the LD single-cell category were linked to severe weather reports, only 5.0% (7 / 140 = 0.050) of storms in the subset were classified as severe. Although the frequency of lightning jumps also decreased within the subset, they remained much more frequent than the occurrence of severe weather at the surface, and thus, produced a large number of false alarms.

An attempt was made to decrease the high FAR values within the subset by increasing the DFRDT threshold required to initiate a jump from 2σ to 2.5σ, 3σ, 3.5σ, and 4σ. By increasing the threshold, it is hypothesized that fewer storms will meet the minimum DFRDT required to trigger a jump. While these thresholds might decrease FAR, it is likely that POD will also decrease as a result of fewer jumps occurring. This

intuitive relationship between FAR and POD was previously documented in Schultz et al. (2009); however, the referenced study did not evaluate a sigma algorithm with a coefficient greater than three. The results of the increased sigma thresholds upon the subset 140 ordinary storms are displayed in Table 15. While the higher threshold total lightning algorithms performed marginally better according to the CSI, there was no practical improvement that might be useful in an operational setting. As hypothesized, POD decreased as the sigma threshold was increased.

Sigma Coefficient	Tot. POD	Tot. FAR	Tot. CSI
2	75.0	94.8	5.1
2.5	75.0	94.0	5.7
3	58.3	94.0	5.5
3.5	58.3	92.6	6.8
4	58.3	91.8	7.4

Table 15. Sigma algorithm performance statistics for the 140 storms occurring on ordinary storm days with SI scores greater than or equal to 50. All quantities were calculated in an identical fashion and expressed in the same units as those in previous tables. Since the pool of 140 storms only produced 12 severe weather events (attributed to 7 unique LD storms) for calculation of POD, some POD values are repeated.

It is evident from Tables 14 and 15 that all mutations of the sigma algorithm evaluated in this study struggled to accurately precede severe weather events produced by LD single-cell thunderstorms with high SI scores. While the 2σ algorithm's performance was unsatisfactory on LD single-cell and LD multicell/supercell days, it nonetheless performed more accurately across the broader range of thunderstorms than when applied to a subset of the smallest, most short-lived, slow-moving, and circular LD single-cell thunderstorms.

6.4.4 Performance of the 2σ Algorithm Relative to Previous Research

As mentioned section 6.4.1, while PODs and lead times calculated in this study compare well to Schultz et al. (2011), FARs were substantially greater under this analysis. Since the definition of the algorithm remained constant for both analyses, the only noteworthy differences between this study and Schultz et al. (2011) are the methods of identifying thunderstorms and assigning flashes to those storms, the total lightning data source, and the type of atmosphere being considered. While the algorithm performed most poorly among the subset of the most disorganized LD storms, it's FAR across all environments strongly disagreed strongly with the values determined by Schultz et al. (2011). Thus, it would seem that either the method of identify storms and assigning flashes, the total lightning data source, or a combination of these two factors is responsible for the discrepancy.

While Schultz et al. (2011) does not detail how its 711 thunderstorms were identified or how flashes were assigned to these storms (though the method is presumably similar to the radar tracking-based techniques of Schultz et al. (2009) or Williams et al. (1999)), it seems safe to assume the identification methodology was significantly different than the cluster-based method utilized here. The highly automated method of clustering flashes into groups may be at least partially responsible for the higher FARs documented in this study. For the sake of operational utility, one would hope that an LJA would be robust to changes in thunderstorm identification and flash appropriation; however, the influence of such decisions should be investigated further to determine the sensitivity of LJA accuracy to storm identification and flash appropriation techniques.

The second possible factor influencing the increased FARs is the ENTLN data source. Schultz et al. (2011) utilized total lightning observations from several regional LMAs and provide sufficient detail regarding the methods by which flashes were identified from VHF source points. In this study, all VHF waveforms had already been grouped into flashes by the ENTLN as explained by Liu and Heckman (2011). Once again, for the sake of operational utility, one would hope that an LJA would be robust to changes in the input data source, especially considering the GLM will represent yet another total lightning observation platform. Future research could seek to calculate LJA accuracy among a common set of thunderstorm between two different total lightning datasets to assess the sensitivity of an LJA to the input data.

6.5 Conclusions

Single-cell thunderstorms are frequent summertime convective phenomena that occasionally endanger human life and property in the form of severe weather. While these ordinary thunderstorms are not consistent producers of severe weather, they do represent a significant summer forecasting challenge for NWS warning coordinators in the Blacksburg NWSFO, and presumably, within other NWSFOs. Recent studies have produced encouraging results suggesting that total lightning jumps might provide a useful operational warning tool toward the impending severity of thunderstorms across a variety of storm environments (Goodman et al. 2005; Schultz et al. 2011).

This study evaluated the performance of the 2σ lightning jump algorithm (Schultz et al. 2009, 2011) in both weakly-sheared and more strongly sheared environments with the purpose of evaluating the transferability of the 2σ algorithm to disorganized

convective regimes. The results corroborate several aspects of previous LJA studies; however, FAR values across both regimes were greater than 85%, with values for the purest LD single-cell storms exceeding 90% - much higher than previously documented (Schultz et al. 2011). Additionally, severe thunderstorms occurring within a weakly-sheared atmosphere appear to more resemble longer-lived multi-cell complexes than discrete single-cell thunderstorms.

If any variation of an LJA is to be incorporated into the warning decision process, its FAR must be greatly reduced. Although such an acceptably low FAR was documented by Schultz et al. (2011), this current analysis was unable to replicate their results. While the 2σ algorithm configuration failed to deliver an acceptable level of accuracy, the statistically significant differences in total flash rate and total DFRDT between severe and nonsevere storms suggest that total lightning behavior can certainly be utilized to help inform forecasters of imminent severe weather. Figure 21c and 21d suggest that 25 fpm could provide an anecdotal threshold differentiating between severe and nonsevere convection though this value is much smaller than the 60 fpm suggested by Williams et al. (1999). While a 10 fpm minimum threshold was required for the algorithm to activate (Schultz et al. 2011), future studies might seek to raise this minimum threshold based on guidance from Figure 21.

While the research question posed by this study dealt solely with the transferability of the algorithm across a broader range of convective regimes, perhaps its most useful conclusions relate to the influence of the data processing techniques upon LJA accuracy. It is suspected that differences in either the methods of identifying

thunderstorms and appropriating flashes or the total lightning datasets is responsible for the large discrepancy in FAR between this analysis and Schultz et al. (2011). Thus, future research might consider isolating the influence of these two factors on LJA performance. This is especially wise considering that all NWS offices have access to ENTLN observations (while few have access to real-time LMA data) and that if the algorithm becomes operationalized, a standard method of identify storms and their associated flashes will be required that optimizes LJA accuracy.

CHAPTER 7

Conclusions

The original research conducted in the preceding chapters successfully adapts emerging technology of total lightning detection to the application of thunderstorm mode classification and lightning jump evaluation. Total lightning flashes observed by the ENTLN between 1 May and 31 August 2012 (Ch. 4) and 2013 (Ch. 5) were clustered into likely thunderstorms and then categorized as either LD single-cell or LD multicell/supercell based on their spatial and temporal characteristics. Days with a majority of LD single-cell storms possessed statistically significant weaker 0000 UTC 0-6 km wind shear than days with a simple majority of LD multicell/supercell storms. This result confirms the traditional expectations that single-cell thunderstorms form in environments characterized by weak wind shear. The environmental expectations for single-cell thunderstorm development were additionally validated by a series of synoptic atmospheric composites comparing LD single-cell days to LD multicell/supercell days.

The results of Chapter 4 encourage the idea that total lightning might well be capable of providing an automated alternative to radar-based classification. The desire of researchers to segregate storms by mode while still considering large sample size necessitates that current storm mode identification efforts benefit from increased automation. However, the methodology introduced in Chapter 4 is preliminary, and requires much refinement and improvement before total lightning can be seriously considered as a substitute for radar-based convective mode identification.

Adding to Chapter 4, Chapter 5 expanded the temporal domain of ENTLN observations to include 2013 in addition to 2012. The subset of storms occurring on LD single-cell days was compared against the underlying terrain to evaluate the topographic influences on single-cell thunderstorm development. EDHSs were hypothesized to host a greater frequency of thunderstorms due to their accelerated heating patterns caused by solar radiation. This hypothesis was confirmed as EDHSs possessed a 37.6% increase in LD single-cell thunderstorm frequency than non-EDHSs at a 15 km resolution of the DEM. These results supported previous work that considered the frequency of convective clouds over terrain (Gambill and Mecikalski 2011; Gibson and Vonder Haar 1990) as well as several studies that analyzed the frequency of radar echoes over variable topography (Kuo and Orville 1973; Outlaw and Murphy 2000).

Chapter 6 built upon the results of Chapters 4 and 5 by analyzing the temporal patterns of all lightning flashes associated with the LD single-cell and LD multicell supercell storms determined in Chapter 5. However, due to a data integrity issue (Ch. 3), it was decided that only 2012 LD storms would constitute proper candidates for further analysis. The 2σ lightning jump algorithm (Schultz et al. 2011) was selected as the definition by which total lightning jumps would be identified. Jumps were subsequently compared to severe weather reports to assess the accuracy of the jumps for operational use. Despite promising results from several previous studies (e.g., Darden at al. 2010; Schultz et al. 2009, 2011; Williams et al. 1999), the performance of the algorithm under this analysis was far from satisfactory.

Ultimately, the purpose of this master's thesis is to assess the utility of total lightning in the diagnosis of single-cell thunderstorm severity. To accomplish the task, the researcher began by developing a systematic method of identifying likely thunderstorms via total lightning data and classifying each storm's convective mode by its spatiotemporal total lightning characteristics (Ch. 4). Once this process was performed on two summers of total lightning data (Ch. 5), it was possible to evaluate spatial distributions of LD single-cell storms (Ch. 5) and assess the capability of the total lightning patterns constituting each storm to accurately signal severe weather manifestation (Ch. 6).

With FARs greater than 80% across all subsets of LD storms considered, it might be tempting to conclude that the algorithm is not fit for operational service under its current definition. However, it is wise to restate the methodological differences between this thesis and those of Schultz et al. (2011). Since the definition of the algorithm remained constant, the only remaining obvious discrepancies are the methods of identifying thunderstorms and appropriating flashes and the total lightning data sources. Since previous literature has not suggested that either of these factors may hold great influence over the 2σ lightning jump algorithm's accuracy, future research should investigate the effect of these two variables.

Though the results of this thesis do not support the operational utility of the 2σ lightning jump algorithm in diagnosing single-cell thunderstorm severity (Ch. 6), there do exist clear differences between the total lightning flash parameters of severe LD storms versus nonsevere LD storms. While the 2σ algorithm was not a satisfactory tool in

highlighting such differences, this thesis does conclude that, with refinement, total lightning patterns may very well offer additional insight into potential single-cell thunderstorm severity. Future research could benefit from considering a larger temporal and spatial domain, developing an variation to the 2σ algorithm that utilizes a higher minimum flash rate prior to the algorithm's activation, and addressing the needed refinements of the storm mode identification methodology from Chapter 4.

References

Austin, P. M., and R. A. Houze Jr, 1972: Analysis of the structure of precipitation patterns in New England. *J. Appl. Meteor.*, **11,** 926-935.

Boccippio, D. J., K. L. Cummins, H. J. Christian, and S. J. Goodman, 2001: Combined Satellite- and Surface-Based Estimation of the Intracloud–Cloud-to-Ground Lightning Ratio over the Continental United States. *Mon. Wea. Rev.*, **129,** 108-122.

Bunkers, M. J., B. A. Klimowski, J. W. Zeitler, R. L. Thompson, and M. L. Weisman, 2000: Predicting supercell motion using a new hodograph technique. *Wea. Forecasting*, **15,** 61-79.

Byers, H. R., and R. R. Braham, 1949: *The Thunderstorm: Report of the Thunderstorm Project.* US Government Printing Office, 287 pp.

Carey, L. D., and Coauthors, 2011: Inter-comparison of lightning trends from ground-based networks during severe weather: applications toward GLM. *2011 Southern Thunder/GLM Users' Conference*, Norman, OK, 11-14

Csirmaz, K., A. Simon, G. Pistotnik, Z. Polyánszky, M. Neštiak, Z. Nagykovácsi, and A. Sokol, 2013: A study of rotation in thunderstorms in a weakly- or moderately-sheared environment. *Atmos. Res.*, **123,** 93-116.

Cummins, K. L., and M. J. Murphy, 2009: An overview of lightning locating systems: history, techniques, and data uses, with an in-depth look at the US NLDN. *IEEE Trans. Electromagn. Compat.*, **51,** 499-518.

Darden, C. B., D. J. Nadler, B. C. Carcione, R. J. Blakeslee, G. T. Stano, and D. E. Buechler, 2010: Utilizing Total Lightning Information to Diagnose Convective Trends. *Bull. Amer. Meteor. Soc.*, **91,** 167-175.

Doswell, C. A., R. Davies-Jones, and D. L. Keller, 1990: On summary measures of skill in rare event forecasting based on contingency tables. *Wea. Forecasting*, **5,** 576-585.

Earth Networks, cited 2012: WeatherBug Confirms Position as Operator of the Fastest, Most Complete Lightning Network [Available online at http://www.earth networks.com/MediaCenter/PressRelease/tabid/118/newsid513/16/Default.aspx.]

Everitt, B., S. Landau, and M. Leese, 2001: *Cluster analysis.* Arnold; Oxford University Press.

Federal Aviation Administration, 2013: Glider Flying Handbook. D. o. Transportation, Ed.

Fierro, A. O., J. Gao, C. L. Ziegler, E. R. Mansell, D. R. MacGorman, and S. R. Dembek, 2014: Evaluation of a cloud-scale lightning data assimilation technique and a 3DVAR method for the analysis and short-term Forecast of the 29 June 2012 derecho event. *Mon. Wea. Rev.*, **142,** 183-202.

Filiaggi, T., 2012: Lightning Jump Evaluation. *RITT Presentation*, T. Filiaggi, Ed., National Weather Service.

Fovell, R. G., and M.-Y. C. Fovell, 1993: Climate zones of the conterminous United States defined using cluster analysis. *J. Clim.*, **6,** 2103-2135.

Fuelberg, H. E., and D. G. Biggar, 1994: The preconvective environment of summer thunderstorms over the Florida panhandle. *Wea. Forecasting*, **9,** 316-326.

Gallus, W. A., N. A. Snook, and E. V. Johnson, 2008: Spring and summer severe weather reports over the midwest as a function of convective mode: A preliminary study. *Wea. Forecasting*, **23,** 101-113.

Gambill, L. D., and J. R. Mecikalski, 2011: A Satellite-Based Summer Convective Cloud Frequency Analysis over the Southeastern United States. *J. Appl. Meteor. Climatol.*, **50,** 1756-1769.

Gatlin, P. N., and S. J. Goodman, 2010: A total lightning trending algorithm to identify severe thunderstorms. *J. Atmos. Oceanic Technol.*, **27,** 3-22.

Gesch, D., G. Evans, J. Mauck, J. Hutchinson, and W. J. Carswell Jr., cited 2013: The National Map—Elevation: U.S. Geological Survey Fact Sheet

Gibson, H. M., and T. H. Vonder Haar, 1990: Cloud and convection frequencies over the southeast United States as related to small-scale geographic features. *Mon. Wea. Rev.*, **118,** 2215-2227.

Gong, X., and M. B. Richman, 1995: On the application of cluster analysis to growing season precipitation data in North America east of the Rockies. *J. Clim.*, **8,** 897-931.

Goodman, S. J., D. E. Buechler, P. D. Wright, and W. D. Rust, 1988: Lightning and precipitation history of a microburst-producing storm. *Geophys. Res. Lett.*, **15,** 1185-1188.

Goodman, S. J., and Coauthors, 2005: The North Alabama Lightning Mapping Array: Recent severe storm observations and future prospects. *Atmos. Res.*, **76,** 423-437.

Guillot, E. M., T. M. Smith, V. Lakshmanan, K. L. Elmore, D. W. Burgess, and G. J. Stumpf, 2008: Tornado and severe thunderstorm warning forecast skill and its relationship to storm type. *24th Int. Conf. on Interactive Information Processing Systems for Meteor., Oceanogr., and Hydrol.*, New Orleans, LA, Amer. Meteor. Soc. [Available online at http://ams.confex.com/ams/pdfpapers/132244.pdf.]

Hallenbeck, C., 1922: The topographic thunderstorm. *Mon. Wea. Rev.*, **50,** 284-287.

Kalkstein, L. S., G. Tan, and J. A. Skindlov, 1987: An evaluation of three clustering procedures for use in synoptic climatological classification. *J. Clim. Appl. Meteorol.*, **26,** 717-730.

Kalnay, E., and Coauthors, 1996: The NCEP/NCAR 40-Year Reanalysis Project. *Bull. Amer. Meteor. Soc.*, **77,** 437-471.

Klitch, M. A., J. F. Weaver, F. P. Kelly, and T. H. Vonderhaar, 1985: Convective cloud climatologies constructed from satellite imagery. *Mon. Wea. Rev.*, **113,** 326-337.

Kuo, J.-T., and H. D. Orville, 1973: A radar climatology of summertime convective clouds in the Black Hills. *J. Appl. Meteor.*, **12,** 359-368.

Liu, C., and S. Heckman, 2011: The application of total lightning detection and cell tracking for severe weather prediction. *91st Amer. Meteor. Soc. Annual Meeting*, Seattle, WA, 1-10

Livingston, J. M., and E. P. Krider, 1978: Electric fields produced by Florida thunderstorms. *J. Geophys. Res.: Oceans*, **83,** 385-401.

Maceachren, A. M., 1985: Compactness of geographic shape - comparison and evaluation of measures. *Geografiska Annaler Series B-Human Geography*, **67,** 53-67.

MacGorman, D. R., D. W. Burgess, V. Mazur, W. D. Rust, W. L. Taylor, and B. C. Johnson, 1989: Lightning Rates Relative to Tornadic Storm Evolution on 22 May 1981. *J. Atmos. Sci.*, **46,** 221-250.

MacGorman, D. R., I. R. Apostolakopoulos, N. R. Lund, N. W. S. Demetriades, M. J. Murphy, and P. R. Krehbiel, 2011: The Timing of Cloud-to-Ground Lightning Relative to Total Lightning Activity. *Mon. Wea. Rev.*, **139,** 3871-3886.

Mallick, S., and Coauthors, 2013: Calibration of the ENTLN against rocket-triggered lightning data. *International Symposium on Lightning Protection*, Belo Horizonte, Brazil

Markowski, P., and Y. Richardson, 2010: *Mesoscale meteorology in midlatitudes.* First ed. Wiley-Blackwell, 407 pp.

Marzban, C., S. Sandgathe, H. Lyons, and N. Lederer, 2009: Three spatial verification techniques: cluster analysis, variogram, and optical flow. *Wea. Forecasting*, **24,** 1457-1471.

Milligan, G. W., and M. C. Cooper, 1985: An examination of procedures for determining the number of clusters in a data set. *Psychometrika*, **50,** 159-179.

——, 1988: A study of standardization of variables in cluster analysis. *J. Classification*, **5,** 181-204.

Montanya, J., and Coauthors, 2009: Study of the total lightning activity in a hailstorm. *Atmos. Res.*, **91,** 430-437.

National Climatic Data Center, cited 2013: Storm Data FAQ

National Weather Service, cited 2012: National Weather Service Mission Statement

Office of Climate, W., and Weather Services, cited 2012: Natural Hazard Statistics. [Available online at http://www.nws.noaa.gov/os/hazstats.shtml.]

Outlaw, D. E., and M. P. Murphy, 2000: A radar-based climatology of July convective initiation in Georgia and surrounding area. *NOAA Eastern Region Tech. Attachment*, **4,** 15.

Rauber, R., J. Walsh, and D. Charlevoix, 2008: *Severe and hazardous weather.* 3rd ed. Kendall/Hunt Publishing Company, 642 pp.

Rudlosky, S. D., and H. E. Fuelberg, 2013: Documenting storm severity in the Mid-Atlantic Region using lightning and radar information. *Mon. Wea. Rev.*, **141,** 3186-3202.

Saaty, T. L., 1994: How to make a decision: the analytic hierarchy process. *Interfaces*, **24,** 19-43.

Schultz, C. J., W. A. Petersen, and L. D. Carey, 2009: Preliminary Development and Evaluation of Lightning Jump Algorithms for the Real-Time Detection of Severe Weather. *J. Appl. Meteor. Climatol.*, **48,** 2543-2563.

——, 2011: Lightning and severe weather: a comparison between total and cloud-to-ground lightning trends. *Wea. Forecasting*, **26,** 744-755.

Shackford, C. R., 1960: Radar Indications of a precipitation-lightning relationship in New England thunderstorms. *J. Meteor.*, **17,** 15-19.

Sloop, C., C. Lui, and S. Heckman, 2014: Analysis of Earth Networks total lightning detection efficiency versus LIS for 2011 through 2013 in North America. *18th Conf. on Integrated Observing and Assimilation Systems for the Atmos., Oceans, and Land Surface*, Atlanta, GA

Smith, B. T., R. L. Thompson, J. S. Grams, and C. Broyles, 2010: Climatology of convective modes for significant severe thunderstorms in the contiguous United States. *Preprints, 25th Conf. on Severe Local Storms, Denver, CO, Amer. Meteor. Soc.*,

Smith, B. T., R. L. Thompson, J. S. Grams, C. Broyles, and H. E. Brooks, 2012a: Convective modes for significant severe thunderstorms in the contiguous United States. Part I: storm classification and climatology. *Wea. Forecasting*, **27,** 1114-1135.

Smith, B. T., T. E. Castellanos, A. C. Winters, C. M. Mead, A. R. Dean, and R. L. Thompson, 2012b: Measured severe convective wind climatology and associated convective modes of thunderstorms in the contiguous United States, 2003–09. *Wea. Forecasting*, **28,** 229-236.

Sreenivasan, H., cited 2012: How 2011 Became a 'Mind-Boggling' Year of Extreme Weather

Stahle, D. W., and M. K. Cleaveland, 1992: Reconstruction and Analysis of Spring Rainfall over the Southeastern U.S. for the Past 1000 Years. *Bull. Amer. Meteor. Soc.*, **73,** 1947-1961.

Stonefield, R., and J. Hudgins, 2006: A severe weather climatology for the WFO Blacksburg, Virginia, county warning area. N. O. a. A. Administration, Ed., Department of Commerce, 19.

Storm Prediction Center, cited 2012: Frequently Asked Questions. [Available online at http://www.spc.noaa.gov/faq/ - 4.1.]

Thompson, R. L., C. M. Mead, and R. Edwards, 2007: Effective storm-relative helicity and bulk shear in supercell thunderstorm environments. *Wea. Forecasting*, **22,** 102-115.

Thompson, R. L., R. Edwards, J. A. Hart, K. L. Elmore, and P. Markowski, 2003: Close proximity soundings within supercell environments obtained from the Rapid Update Cycle. *Wea. Forecasting*, **18,** 1243-1261.

Trapp, R. J., S. A. Tessendorf, E. S. Godfrey, and H. E. Brooks, 2005: Tornadoes from squall lines and bow echoes. Part I: Climatological distribution. *Wea. Forecasting*, **20,** 23-34.

Weisman, M. L., and J. B. Klemp, 1982: The dependence of numerically simulated convective storms on vertical wind shear and buoyancy. *Mon. Wea. Rev.*, **110,** 504-520.

——, 1984: The structure and classification of numerically simulated convective storms in directionally varying wind shears. *Mon. Wea. Rev.*, **112,** 2479-2498.

Williams, E., and Coauthors, 1999: The behavior of total lightning activity in severe Florida thunderstorms. *Atmos. Res.*, **51,** 245-265.

Williams, E. R., M. E. Weber, and R. E. Orville, 1989: The relationship between lightning type and convective state of thunderclouds. *J. Geophys. Res.: Atmos.*, **94,** 13213-13220.

Wind, Y., and T. L. Saaty, 1980: Marketing applications of the Analytic Hierarchy Process. *Management Sci.*, **26,** 641-658.

Witt, A., M. D. Eilts, G. J. Stumpf, E. D. W. Mitchell, J. T. Johnson, and K. W. Thomas, 1998a: Evaluating the Performance of WSR-88D Severe Storm Detection Algorithms. *Wea. Forecasting*, **13,** 513-518.

Witt, A., M. D. Eilts, G. J. Stumpf, J. T. Johnson, E. D. W. Mitchell, and K. W. Thomas, 1998b: An Enhanced Hail Detection Algorithm for the WSR-88D. *Wea. Forecasting*, **13,** 286-303.

Zhang, T. F., X. Duan, J. Zhang, L. Y. Yin, and L. Liu, 2013: Characteristics and relations of lightning and radar echoes for strong convective rainstorms in Yunnan. *J. Trop. Meteor.*, **19,** 188-196.